TECHNICAL MEMORANDUM

327

Assessment of the ECMWF model cloudiness and surface radiation fields at the ARM-SGP site

J-J.Morcrette

Research Department

January 2001

European Centre for Medium-Range Weather Forecasts
Europäisches Zentrum für mittelfristige Wettervorhersage
Centre européen pour les prévisions météorologiques à moyen

Assessment of the ECMWF Model Cloudiness and Surface Radiation Fields at the ARM-SGP Site

Jean-Jacques Morcrette

European Centre for Medium-Range Weather Forecasts, Shinfield Park, Reading Berkshire RG2 9AX, United Kingdom

Abstract

The cloud and radiation fields produced by the operational ECMWF forecasts are assessed using observations from the Atmospheric Radiation Measurement Program (ARM) South Great Plains (SGP) site over the April-May 1999 period.

Over the first 36 hours of the forecasts, most of the model fields, taken over a 24-hour time window (either 0-24, 6-30, or 12-36-hour) are generally consistent with each other. Comparisons of model fields taken from any such 24-hour time window with observations are therefore representative of the quality of the ECMWF model physical parametrizations.

The surface radiation fluxes are assessed separately for clear-sky, overcast, and whole-sky situations. For clear-sky fluxes, differences between model and observations are linked to differences in humidity and temperature profiles, the characterization of aerosols, and systematic errors in the shortwave radiation scheme.

Model cloud occurrences and boundaries over the Central Facility are compared with similar quantities derived from radar and micropulse lidar observations. Model cloud water is tentatively assessed through comparisons with the radar reflectivity measurements. Systematic deficiencies in the surface radiation fields in presence of clouds are discussed with respect to differences between the model and observed cloud characteristics.

Given the T_L319 resolution of the ECMWF model at the time of the comparisons, both the day-to-day and temporal variability within-the-day are reasonably well captured by 24-hour forecasts including cloud-radiation interactions with 1-hour time resolution. However, most of the differences with observations can be traced back to either deficiencies in the clear-sky shortwave radiation scheme, or problems in the cloud fraction and/or cloud water content.

1. Introduction

The top-of-the-atmosphere (ToA) radiation longwave (LW) and shortwave (SW) radiation fields produced by general circulation models (GCMs) have been assessed globally since, in the mid-60's, satellites started to measure radiances (e.g., Holloway and Manabe, 1971 using the radiation budget from Vonder Haar, 1969). Contrary to ToA radiation, an assessment for surface radiation fields has appeared much more recently with the production of the first satellite-derived surface radiation climatologies (*Darnell et al.*, 1992; *Laszlo and Pinker*, 1993; *Li and Leighton*, 1993). Even so, the quality of such surface radiation climatologies is still questioned, due to processes either inadequately known and/or accounted for in the retrieval (LW absorption by water vapour continuum, LW and SW aerosol effects, "anomalous" SW absorption).

In the recent past, good quality surface radiation measurements such as those screened from the Global Energy Balance Archive (*Ohmura and Gilgen*, 1993) have usually been preferred for the evaluation of the surface radiation fields produced by GCMs. *Garratt and co-authors* (1994, 1996, 1998), and *Wild and co-authors* (1995, 1998a, 1998b, 2000) have looked at the biases produced by GCMs and operational analyses, and their implications for climate modelling. However, such studies are usually carried out on a monthly time scale, with a mix of clear-sky and cloudy conditions. Distinction between systematic and random errors has not been clearly stated: the deficiencies in the surface radiation fields identified by these studies have not been readily ascribed, in the case of non-cloudy situations, to model deficiencies in the radiation codes, in temperature and humidity profiles, or to the improper or lack of account for aerosols. In the case of cloudy situations, the

deficiencies previously noted have been inadequately characterized in terms of the cloudiness produced by the model (i.e., cloud fraction, cloud base height, optical thickness, cloud condensed water). Moreover, in these comparisons, the information about these profiles is usually incomplete, so that a thorough assessment is difficult.

In the past, a number of in-situ measurement campaigns have provided simultaneous observations of some of the cloud-radiation related parameters over a given location, usually over a rather short period of time. Unfortunately, these measurements have not been generally used to assess the quality of the model simulations and operational analyses.

The much wider set of observations of the Atmospheric Radiation Measurement program (ARM: *Stokes and Schwartz*, 1994) provides better definition of the surface radiation budget and its governing parameters, allowing more constraints in the verification of the fields produced by a large-scale model (*Beesley et al.*, 2000; *Mace et al.*, 2000). In this study, two months of measurements over the ARM-South Great Plains site (SGP) in Oklahoma are used to evaluate most of the cloud-radiation aspects in the ECMWF model. The observational and model data are discussed in section 2. Results for the model grid point corresponding to the SGP Central Facility (CF) are presented in section 3. The sensitivity of the surface radiation fields to details of the parametrization is presented in section 4. Discussion and conclusions are presented in section 5.

2. Methodology

2.1 Observational and model data

The study covers the whole months of April and May 1999. A spring period was preferred because spring had, in the past, not been a particularly good period for ECMWF forecasts. Moreover, for somewhat average conditions of temperature and humidity, a large temporal variability can be expected at the latitude of the ARM-SGP site (Lamont, Oklahoma, 36.605°N, 97.485°W), depending on the flow direction of the prevalent air mass. In the following, use is made of measurements by the observational systems located at the Central Facility. These are defined together with the measured parameters in Table 1.

The ECMWF fields correspond to outputs every one hour for all 48-hour forecasts starting 24-hours apart between 19990331 12UTC and 19990531 12 UTC. The analyses from which the forecasts were started are obtained through a 4-D variational assimilation of all the observations during a 6-hour window centered around the analysis time (*Rabier et al.*, 1998; *Mahfouf and Rabier*, 2000). The model used in this study is the so-called cycle 23R1 of the ECMWF Integrated Forecast System, operational between 27 June and 11 November 2000. Among the modifications introduced with cycle 23R1 are the replacement of the previous longwave scheme (*Morcrette*, 1991; hereafter referred to as M91) by the Rapid Radiation Transfer Model (*Mlawer et al.*, 1997) and the introduction of a tiling scheme for the surface processes (*van den Hurk et al.*, 2000). The M91 longwave (LW) scheme included cloud effects using maximum-random overlap of effective cloud layers through an effective emissivity approach. The ECMWF version of the RRTM LW scheme (*Morcrette et al.*, 1998) also includes a maximum-random overlap assumption but keeps the cloud fraction and cloud optical thickness as two separate quantities.

The rest of the package of physical parametrizations (*Gregory et al.*, 2000) includes the SW radiation scheme originally developed by *Fouquart and Bonnel* (1980) and revised by *Morcrette* (1993). The cloud optical

properties are based on *Ebert and Curry* (1992) for ice clouds and on *Fouquart* (1987) and *Smith and Shi* (1992) for water clouds. All cloudy fluxes are computed from cloud optical thicknesses derived from the prognosed liquid and ice cloud water content weighted by a 0.7 inhomogeneity factor following *Tiedtke* (1996). The switching between deep or shallow convection was modified in December 1997 (cycle 18R6) from a test on the moisture convergence to one based on the depth of the convection (*Gregory et al.*, 2000). The dynamical part of the model includes the two-time-level semi-lagrangian scheme (*Hortal*, 2000) on a linear grid of *Hortal and Simmons* (1991).

The prognostic cloud scheme (*Tiedtke*, 1993) represents both stratiform and convective clouds, and their time evolution is defined through two large-scale budget equations for cloud water content and cloud fractional cover. This scheme links the formation of clouds to large-scale ascent, diabatic cooling, boundary-layer turbulence, and their dissipation to adiabatic and diabatic heating, turbulent mixing of cloud air with unsaturated environmental air, and precipitation processes. The results presented in the following sections are obtained with the scheme used operationally for global forecasts and analyses. It includes the original formulation of the fallout of cloud ice of *Tiedtke* (1993). It only differs from Tiedtke's original formulation through a new precipitation/evaporation (*Jakob and Klein*, 2000), which explicitly accounts for the vertical distribution of cloud layers and allows the cloud overlap assumption to be applied consistently with what is done for the radiative computations.

In the study presented here, the T_L319 L60 model (about 40 km horizontal resolution and 60 levels in the vertical) is run with a 20-minute time-step. The physical grid corresponds to 0.5625^o (about 60 km at the equator) and keeps roughly the same dimension going towards the poles thanks to the linear grid (*Simmons and Hortal,* 1991). The 60-level vertical resolution includes about twelve levels between the surface and the average top of the planetary boundary layer (PBL). The full radiation computations (i.e., those using updated cloud fraction and cloud water; *Morcrette*, 2000) are called every hour. This is the only difference with the operational configuration, which instead calls the full radiation computations every hour during the first 6 hours, and every 3 hours thereafter.

With regards to the analysis of conventional meteorological observations, over the continental U.S., surface information is obtained from the network of synoptic stations, and upper air profiles are derived from the conventional radiosoundings.

A discrepancy exists between the model surface height (391 m) and the true orography (318 m). In their comparison of monthly mean surface radiation fields with observations, *Wild et al.* (1995) simply used a height correction of 2.8 W m^{-2} (100 m)$^{-1}$, which was originally derived from measurements at different heights in the Alps. In contrast to *Wild et al.* (1995), the model fields are not corrected for the 73 m discrepancy between the model and actual orographic heights.

2.2 Methodology of comparisons

One of the vexing questions when comparing outputs from a forecast model with observations concerns the dependence on the forecast range of such comparisons. In principle, one could expect the best results as close as possible to the analysis time, but in practice, the existence of some imbalance between the analyzed fields and the fields that the model would create in a free running mode, leads to a rapid transient response of the model at the start of the forecast (spin-up or down). Such an imbalance has, in the past, been particularly

obvious in the humidity field (*Illari*, 1987). In order to assess the impact of this model feature, various fields have been compared over 24-hour windows from different forecast ranges. For each of the windows used in the comparisons shown hereafter (0-24, 6-30, 12-36 hours), the 24 hourly values are used to build the time-series for a given day, and the 30 or 31 such daily time-series are then put together to create a month (April or May). Figures 1 to 4 present, over the month of April 1999, the evolution of different fields (surface pressure and temperature, total and low-level cloudiness in Fig. 1, vertically integrated water vapour and cloud water, surface downward shortwave and longwave radiation in Fig. 2), for different 24-hour time windows within the 36-hour forecast range. Table 2 presents the monthly averages and standard deviations of a number of parameters over 61 days covering the months of April and May 1999. Whereas the overall agreement between the different forecast windows (00-24, 06-30, 12-36 hours) is good for the surface pressure and skin temperature, parameters linked to the moisture distribution (total and low-level cloudiness, and resulting surface and ToA radiative fluxes, surface latent heat flux) display slightly less consistency. However, on the period April-May 1999, the average surface downward LW and SW fluxes taken at different ranges do not differ by more than 3.4 Wm^{-2}.

When comparing model outputs with observational measurements, a number of methodological points need to be addressed to put the results into context. These are related to the model horizontal resolution and the spatial scales actually represented by the model, but also to the model temporal resolution and the averaging process required on observations to get consistent comparisons.

In the following sections, the comparisons will be shown between the 00-24 hour forecast values and the observations, all averaged over 1-hour intervals, to be consistent with the timestep for the full radiation computations. As can be seen from the last column in Table 1, the averaging will differ widely from one observation system to the other. For radiative fluxes, surface pressure and skin temperature, the averaging is carried out taking all values after rejecting the (few) unrealistic values. The same procedure has been applied to measurements from the MicroWave Radiometer. The vertically integrated cloud water measurements are obviously contaminated by precipitation and/or presence of condensation on the optics. Thus, the so-called "wet" index is presented averaged over one hour, to point out the instances where measurements are unreliable (Fig. 4).

For cloud base height, cloud boundaries and cloud mask, a simple average over one hour, excluding non-cloud (clear-sky) values is carried out. The liquid water equivalent reflectivities from the radar (Ze) are first translated into liquid water content (LWC) using a given Ze-LWC relationship (see Appendix). The averaging over height and time is then performed on these liquid water contents to put the observations into the same vertical grid and time frame as the model outputs. Finally the resulting LWC are translated back to dBZ using the related LWC-Ze relationship.

3. Comparisons at the Central Facility

Two related questions need to be answered: how consistent is the observation of a given quantity, and what is the quality of the model representation of that quantity? In the following, when two measurements of the same quantity are available from neighbouring instruments within the Central Facility, their comparison enables, somewhat empirically, the range of uncertainties in the observations to be defined. Then given that background information, it is then possible to look at how successful the model is at simulating this quantity.

3.1 Surface pressure and temperature

The surface pressure measured by the Energy Balance Bowen Ratio system at station E13 (Central Facility) and the corresponding synoptic measurement (SMOS) are compared, for the month of April 1999, with the ECMWF model 00-24-hour forecasts in Figure 3 (top). There is a very good agreement between observations and model in surface pressure, not surprising given that the synoptic observations of pressure are usually assimilated by the ECMWF system. Over the 979 hours for which two independent measurements of surface pressure are available during April-May 1999, the correlation between the C1 and E13 observations is 0.998 and the mean bias is 0.7 hPa (see Table 3). Whatever the forecast range, the model pressure is within the observed range defined by the C1 and E13 observations.

From measurements of the upward LW radiation by the downward looking pyrgeometers (SIRS C1 and E13), an equivalent surface skin temperature was derived from $F^{up} = \sigma T^4$ and compared to the equivalent quantity diagnosed the model skin temperature, surface downward LW radiation and surface emissivity in Figure 3 (bottom). The agreement between the two neighbouring observations of the equivalent surface skin temperature is poorer than for surface pressure, reflecting the possible influence of the soil moisture on the surface emissivity (see Table 3). This also shows when comparing with the model equivalent skin temperature (SKT): over the first half of April, the model maximum SKT is often too low by 2 to 3 K, and the nighttime minimum too high by 3 to 4 K, therefore indicating too small a diurnal cycle for the model skin temperature.

3.2 Total column water vapour and cloud water

The model total column water vapour (TCWV) and total column cloud water (TCCW) are compared over April 1999, with quantities derived from Microwave Radiometer (MWR) observations in Figure 4 (top and bottom, respectively). The agreement in TCWV is quite good, specially for the low values. For the highest values, some uncertainty might exist in the observations, due to moisture condensing on the observing device. The periods over which such a problem occurs are given by the wet index at the bottom of Figure 4a, and top of Fig 4b, with grey and black shading depending whether less or more than 30 mn within the 1-hour period shows an active index in the original 20-s measurements. A comparison was also made with the vertically integrated water vapour derived from the humidity information in the radiosoundings at Lamont (OK), close to the Central Facility. There is an overall good visual agreement. However as seen from Table 3, over the 142 radiosoundings in the April-May period, the TCWV derived from the radiosonde is slightly smaller (by 1.7 kg m^{-2}) than the MWR-derived value.

The total column cloud water (TCCW) (Fig. 4 bottom) is much more difficult to assess. The model TCCW includes both the liquid and ice water, whereas the retrieved TCCW based on the difference between observations at 23.8 and 31.4 GHz is really cloud liquid water only. The peaks in the observations obviously correspond to clouds above the MWR. They are also usually flagged as wet, so the observations are likely to include precipitation.

3.3 Downward radiation

The corresponding surface downward SW and LW radiation (referred to as Surface Solar Radiation Downward, SSRD, and Surface Terrestrial Radiation Downward, STRD, within the ECMWF model and archive) are presented in Figure 5 (top for SSRD, bottom for STRD) as measured from two sets of radiometers

located at the Central Facility (C1 and E13) and as represented by the model forecasts. Table 3 presents the regression statistics between these two sets of measurements over the April-May period. For all the time slots for which both the E13 and C1 measurements are available over the April-May period, the correlation between the two stations is better than 0.999 for both SSRD and STRD. Some uncertainty arises from the (small) negative values usually reported by the pyranometers during nighttime. In Table 3, statistics for SSRD are reported three times, the first set corresponding to all observations during the period, the second set to all observations with nighttime values set to zero, and the third set to daytime observations only. Over the 2-month period of the observations, the difference between the first two approaches is at most 2.5 Wm^{-2}. In both cases, the correlation is practically unity, and the slope higher than 0.998. Therefore, the slight disagreement between these two approaches is unlikely to be of concern for evaluating the model behaviour.

In clear-sky atmosphere, the STRD is between 240 and 290 Wm^{-2}. Only when clouds are present, does STRD get over 300 Wm^{-2}, with the values over 360 Wm^{-2} corresponding to the presence of low level cloudiness. There is a reasonable agreement between model and observed STRD (Fig.7, bottom), reflecting the ability of the model to produce the cloud events at the right time, with cloud base close to the proper height.

A more detailed assessment of the behavior of the schemes in clear-sky and cloudy conditions is next carried out.

From the 1464 (=61 days x 24) one-hour slots in April-May 1999, 168 clear-sky situations have been extracted (only 164 such situations are for daytime conditions, and are thus used for the SW). This extraction is based on the following set of conditions: a model total cloud cover < 1%, no return from the Multi-Mode Cloud Radar (MMCR), no cloud base from the Micropulse Lidar (MPL), and a zero wet index from the Microwave Radiometer (MWR). Table 4 presents the statistics of the comparisons for TCWV, STRD and SSRD. Over this set of profiles, there is a very good agreement between the MWR-observed and model TCWV and STRD (Figure 6). The agreement for STRD is within the range obtained when comparing C1 and E13 SIRS measurements. In contrast, even on these selected clear-sky cases, the model SSRD overestimates the observed SSRD by 31.2 Wm^{-2} over the 164 daytime situations. This reflects a likely bias in the SW radiation scheme or an improper specification of the aerosol optical thickness (see section 4).

In the presence of cloudiness, the discrepancies between model and observed surface radiation fluxes are as likely to come from incorrect atmospheric profiles, incorrect definition of the cloud parameters (cloud base height and optical properties) produced by the forecasts as from the radiation schemes used in the model. Therefore a set of 59 overcast situations (25 during daytime are used for SSRD) has been extracted, for which the model total cloud cover (TCC) is > 99%, with presence of clouds during all intervals making the one-hour slot in the MMCR, BLC and MPL observations. Results are presented in Figure 7. These cases show an agreement on both the cloud cover and the cloud base height. However, the comparison between MWR-observed and model TCWV is certainly affected by moisture condensating (dew) or precipitating on the observing device. The agreement in STRD is again good (with a 2 Wm^{-2} model overestimation). Again, the model SSRD overestimates the observed SSRD by 26.4 Wm^{-2}. The overestimation is consistent with the deficiency already seen for the SW radiation scheme in clear-sky conditions, but problems in the definition of the cloud optical parameters (optical thickness in particular) cannot be ruled out and are as likely to increase as decrease the clear-sky error.

Finally, Figure 8 displays the comparisons between model and observed downward radiation over the two months. The last two lines in Table 4 gives the corresponding statistics for all possible comparisons for surface radiation over the two months. Over the 1436 LW comparisons (Figure 8, top), the model underestimates the observations by 2 Wm^{-2}. The SW comparisons (figure 8, bottom) are restricted to 821 daytime comparisons and show a 17 Wm^{-2} overestimation by the model.

The net radiation (SW^{down} - SW^{up} + LW^{down} -LW^{up}) is presented in Figure 9, for April 1999, as produced by the model, and measured by the Energy Balance Bowen Ratio system at station E13. In the model, the often large overestimation of the SSRD, the slight underestimation of STRD, and the too large skin temperature at night all contribute to the signature in Figure 9. The model produces too much energy input to the surface during daytime, and too much energy output from the surface at night.

3.4 Cloudiness

The temperature and humidity in the first 3000 m above the surface are presented for the ECMWF model in the top panels of Figures 10 and 11, over the month of April 1999. The bottom panels in Figs 10 and 11 are the differences between the model values and the temperature and humidity derived from the AER interferometer (AERI). There is an overall good agreement between model and observations, with the range of differences going from -11.0 to 11.6 K for temperature and from -5.2 g kg^{-1} to 8.3 g kg^{-1} for humidity. However, the average bias over the first 3000 m of the atmosphere varies between -1.6 K at the surface and 0.7 K at 3000 m for temperature, and between -0.2 g kg-1 at 300 m and 0.3 g kg-1 at 1800 m.

The capability of the ECMWF model to produce cloudiness at the proper time and height can be also judged by comparing the model cloud fraction with a so-called cloud mask produced from radar measurements and/ or the height of clouds detected by the micropulse lidar (MPL) or the Beaufort Laser Ceilometer (BLC). Figure 12 presents the cloud base height from the model and measured by the Beaufort Laser Ceilometer. When a large amount of clouds, with substantial low-level cloudiness, is present (2-3, 7, 13-14, 24-25 April), the agreement for cloud base height between BLC measurements and the model is generally good. At other times, the agreement is much poorer, and the cloudiness derived from MMCR measurements often does not support the BLC measurements. The vertical distribution of clouds produced by the ECMWF model forecasts for April 1999 is shown in Figure 13 (top panel), together with the cloud mask derived from MMCR measurements using *Clothiaux et al.* (1995)'s algorithm (Fig. 13, bottom panel). Another cloud mask derived from MMCR measurements using Campbell et al. (1995)'s algorithm was also compared with the model and found to lead to similar conclusions.

The vertical distribution of the model cloud ice and liquid water content is presented in Figure 14a and b, respectively. In the ECMWF model, the distinction between liquid and ice water is made based on temperature using a relationship by *Matveev* (1984). It includes a mixed phase between 0 and -23 ^{o}C, seen as an overlap between the two distributions in Figs. 14.

A Ze-reflectivity simulated using IWC-Ze and LWC-Ze relationships from the model IWC and LWC fields of Fig. 14, is presented in Figure 15 (top panel). Details of the procedure follows *Beesley et al.* (2000) and are given in the appendix. The corresponding Ze-reflectivity derived from MMCR measurements by *Clothiaux et al.* (2000) are presented in the bottom panel of Figure 15. The effect of heavy precipitation on the radar

reflectivity data can be seen on the 2nd, 7th, 13th and 24th of April. The observed reflectivity saturates at these times corresponding to a wet index of 1 in the MWR measurements.

The comparison of the two panels in Fig. 15 shows that, in terms of reflectivity, the model is in the ball park of the measurements, particularly for the higher-level (ice) clouds. The results are obtained using the IWC-Ze relationship of *Atlas et al.* (1995) for a 100 μm equivalent particle diameter Do, within the range 60-120 μm diagnosed by the model from temperature following *Matveev* (1984). However, as seen in the appendix, differences up to several dBZ exist between the various IWC-Ze relationships or when Do is allowed to vary between 100 and 900 μm in Atlas et al.'s relationships. So the obtained agreement between model and observations cannot be taken as a sure proof of the adequacy of the model cloud ice water content.

For liquid water clouds, the agreement between the various theoretical relationships is much better, so a disagreement between model and observations is likely to indicate a problem in the distribution of the model cloud liquid water content. As seen in the appendix, the LWC-Ze curves remain within 2 dBZ of each other. The agreement is down to 1 dBZ for Frisch et al.'s relationships when the particle number concentration varies between 150 and 900 cm^{-3}, which correspond to the concentrations implicitly assumed for ocean and land in the ECMWF model. A comparison of the lower parts of clouds in Figure 15 indicates that, for liquid water clouds, the model reflectivity is generally too low.

4. Sensitivity to modelling assumptions

The results presented in the previous section had been obtained with a recently operational representation of the physical processes in the ECMWF model. In the following, clear sky and cloudy profiles are considered separately, and the surface radiation fluxes are studied in terms of their sensitivity to the various versions of the radiation codes available at ECMWF, and the impact of various representations of the aerosols and of the cloud optical properties.

4.1 Radiation codes

Since 27 June 2000, the ECMWF forecast system has been using the Rapid Radiation Transfer Model (RRTM, *Mlawer et al.*, 1997; *Morcrette et al.*, 1998) for its LW computations. Before that date, the operational forecasts were using the LW parametrization of *Morcrette* (1991, M91_LW in Table 5). Also in June 2000, the spectral resolution of the SW radiation scheme was changed from two spectral intervals (0.25-0.69-4.00 μm) to four spectral intervals (0.25-0.69-1.19-2.38-4.00 μm). Table 5 presents a comparison of the downward LW and SW radiation fluxes for the different model configurations, RRTM vs. M91 in the LW, SW4 vs. SW2 in the SW, for whole- and clear sky atmospheres. The better representation of the water vapour continuum absorption in RRTM leads to a 6.3 Wm^{-2} increase in the clear-sky surface downward LW radiation. The impact of changing the number of spectral intervals (from 4 to 2) in the near-infrared part of the spectrum is very small for clear-sky SW radiation (a 0.4 Wm^{-2} decrease in the daytime only average). The impact is larger for cloudy conditions (-2 Wm^{-2} when averaged over daytime only).

4.2 Representation of aerosols

The ECMWF model is operationally run with an annually averaged climatological distribution of aerosols, first designed by *Tanre et al.* (1984). In the present model configuration, five types of aerosols are considered,

four with a geographical variation (maritime, continental, urban and desert aerosols), the fifth one, a stratospheric background aerosol, is included with a homogeneous horizontal distribution. Table 5 presents the effect of this climatological aerosol on the downward flux above the ARM-SGP site. With both the pre- and the post-27 June radiation codes (pre: M91_LW+SW2; post: RRTM+SW4), the aerosols would contribute 0.3 Wm^{-2} to both the clear-sky (SDLWC=surface downward longwave clear) and cloudy (SDLWT=surface downward longwave total) LW fluxes, and about -29 and -23 Wm^{-2} to the clear-sky (SDSWC=surface downward shortwave clear) and cloudy (SWSWT=surface downward shortwave total) SW fluxes.

4.3 Cloud optical properties

In the operational radiation scheme, the water cloud optical properties are defined from *Smith and Shi* (1992) in the LW, and *Fouquart* (1987) in the SW. The effective radius for water clouds is specified as 10 μm over land. For ice clouds, optical properties are taken from Ebert and Curry (1992) in both the LW and SW. Table 6 compares for the month of April, the surface downward fluxes, computed with the same radiation schemes including different sets of cloud optical properties. Water cloud optical properties are defined from *Savijarvi and Raisanen* (1997) in the LW (SR97), and *Slingo* (1989) in the SW (AS89). Ice cloud optical properties are taken from *Fu and Liou* (1993) in the LW, and *Fu* (1996) in the SW. The results presented in Table 6 are obtained using the same profiles of temperature, humidity, cloud fraction and cloud liquid and ice water, to concentrate on the impact of the cloud optical properties. The impact of the various formulations is quite small: the change in SDLWT is smaller than 0.2 Wm^{-2} when concentrating on the cloudy situations. Similarly, the change in SDSWT is smaller than 10 Wm^{-2} for the daytime only cloudy situations. When repeating the calculations with profiles obtained with the various formulations for cloud optical properties interactive in the model, the differences are similar or smaller.

Table 7 presents results obtained with the effective radius of water clouds diagnosed from the cloud liquid water content following *Martin et al.* (1994) for four different concentrations of cloud condensation nuclei (300, 600, 900, and 1200 cm^{-3}). The impact in the LW is negligible as clouds when present are essentially black for computing the surface downward LW flux. However, for the surface downward SW flux, a larger concentration of cloud condensation nuclei (CCN) for the same condensed water leads to smaller droplets, and more effective scattering of SW radiation. A 10 Wm^{-2} decrease in surface downward shortwave radiation, computed for daytime only cloudy situations, is seen when CCN concentration is changed from 300 to 1200 cm^{-3}, a range typical of continental conditions according to *Martin et al.* (1994). Thus the major uncertainty in the modeling of the radiative properties of warm clouds is in the specification of the effective radius via the number concentration of droplets.

5. Discussion and conclusions

From comparisons with surface radiation measurements, *Wild et al.* (1998a, b) have shown the surface radiation fluxes in the ECMWF Re-Analysis of the 1979-1993 period (now called ERA15: *Gibson et al.*, 1997) to be in error, with generally too small downward LW radiation and too high SW downward radiation. However, these comparisons carried out on monthly means did not permit to disentangle the reasons for such errors. In this study, the various measurements carried out at the Central Facility of the ARM-SGP site are used together to pinpoint the deficiencies in the representation of cloud and radiation fields of a recent ECMWF model and relate them to errors in the surface fluxes.

First, an empirical level of uncertainty in the measurements of the various parameters affecting surface radiation is defined by looking at simultaneous measurements of the same parameters by different instruments. The overall consistency in the measurements is such that most of the differences between observations and model prediction can be ascribed to model deficiencies.

Comparisons of model-produced parameters with relevant observations show the model to be successful at producing the gross features of the atmosphere. A number of positive and negative points are identified when the ensemble of observations are taken together to check most of the model parameters describing the cloud-radiation interactions. In the absence of precipitation, the forecast total column water vapour (TCWV) is in good agreement with microwave measurements of the TCWV. When precipitation occurs, the observed TCWV is likely to be affected by the presence of liquid water whose effects on the TCWV measurements are difficult to quantify. When there is a good agreement in TCWV, the error in clear-sky surface LW radiation appears to fall within the range of uncertainties of the measurements. When model and observed clouds are overcast, and there is an agreement on the height of the cloud base, the model and observed surface downward longwave radiation (STRD) are within a few Wm^{-2} from each other. Overall, the current LW radiation scheme (RRTM) has improved over the previous parametrization (M91) used for ERA15.

This is not the case for the SW radiation. A bias in clear-sky SW radiation, possibly linked to an inadequate definition of the aerosols, but more certainly to an outdated parametrization (slightly underestimated water vapour absorption, and inadequate separation between the UV and visible radiation transfer) leads to a model surface downward shortwave radiation (SSRD) larger than the observed one, for all sky conditions. In ERA15, the overestimation of SSRD in clear-sky atmospheres was thought to be linked to the two-interval spectral structure of the SW radiation scheme (*Morcrette*, 1991). The present version of the scheme now has four spectral intervals and still shows a similar overestimation. The better spectral description has slightly improved the near-infrared absorption by clouds. A revised SW scheme based on the most recent spectroscopic data and including a proper separation of the UV and visible band is under development and will be reported in another paper.

Dong et al. (2000) recently studied the seasonal variability in the characteristics of the low-level water clouds above the ARM-SGP site, particularly in the effective radius size and cloud-droplet number concentrations (CDNC). They showed a factor 2 increase in CDNC in winter relative to summer conditions. Independently of the quality of the model cloud water content, the effective radius of the model water cloud droplets, presently specified at 10 μm, is likely to contribute to the underestimation of such a variability in the shortwave radiation fields.

The net surface radiation budget shows a deficient diurnal cycle, with too large input (by 20-30 Wm^{-2}) to the surface during daytime, and too large energy loss (by a similar amount) during nighttime. This problem is linked to the deficiencies discussed above, and to the representation of the cloudiness.

Information from the Multi-Mode Cloud Radar was used for validating the model cloudiness. As already shown in this and other studies (*Mace et al.*, 1998; *Miller et al.*, 1999), the ECMWF cloud scheme is able to represent the gross features of the cloudiness in terms of presence and vertical distribution of the cloud layers. However, the cloud water content is a quantity for which there has been, up to now, very few direct measurements allowing a detailed model validation. A tentative assessment of the vertical distribution of the model cloud water content has been carried out in this study. Given the many uncertainties in the relationships

between cloud water content and radar reflectivity, rising mainly from the definition of the particle effective diameter, we preferred simulating directly the radar reflectivity to retrieving a cloud water from the measurements. When using IWC-Ze and LWC-Ze relationships for which the implicit cloud microphysical parameters are consistent with the model values, a reasonable agreement between model-simulated and radar-observed reflectivity particularly for higher-level clouds. For liquid water clouds, the model-simulated reflectivity is usually too small. This might partly be due to an inaccurate effective radius, as tests with a diagnosed effective radius or different particle number concentrations appear to have a large effect on both the cloud reflectivity and the SSRD underneath such clouds.

It must be pointed out that, for high clouds, the good visual agreement seen in Figure 15 is not a proof that the ECMWF model cloud ice water is realistic, as the equivalent radius assumed for the particles might be different from reality. This is the only statement that can be made in absence of an observational constraint on this parameter.

Such a verification against observations of most of the model parameters relevant for the cloud-radiation interactions could be carried out at the two other ARM sites (Tropical West Pacific and North Slope of Alaska). It could also be carried out at the ARM-South Great Plains site for different seasons, as observations have shown the cloudiness to have markedly different characteristics in summer and winter (*Dong et al.*, 2000).

In the future, PICASSO/CENA and CloudSat will provide, from satellite platforms, a rather equivalent set of radar and lidar measurements of clouds for the purpose of determining their microphysical and radiative properties. This should allow a powerful check of the model-generated cloudiness, including its vertical distribution, on a global scale.

APPENDIX: REFLECTIVITY FROM THE MULTI-MODE CLOUD RADAR AND THE MODEL CLOUD WATER CONTENT

In this study, measurements from the Multi-Mode Cloud Radar are used to evaluate the model cloudiness following closely the approach used by *Beesley et al.* (2000) with the SHEBA dataset. MMCR is a 34.86 GHz (8.66 mm, K_a-band) radar. It has been extensively described in *Clothiaux et al.* (1999, 2000). Here we summarize the arguments used in the processing of ice and/or liquid water content from the observed radar reflectivities.

To get the relationship between the radar reflectivity and the cloud water content, we consider the Rayleigh approximation to the Mie scattering theory, i.e., that the diameter D of the particle must be small in comparison to the radar wavelength λ. From *Marshall and Gunn* (1952), we also assume that the radar back scattering cross section of a small non-spherical particle is equivalent to that of a sphere of the same mass, provided that the particle has the weak dielectric properties of a substance such as ice.

We assume that the particle size distribution follows a distribution of the form

$$N(D) = A\, D^{\beta} \exp(-b\, D)$$

where D is the diameter, β is the shape parameter (varying between 0 and 3), with b =1/Do, the inverse of the mode diameter of the distribution, and A is related to No/ Do^{β}, with No the number concentration. According to Kosarev and Mazin (1990), $\beta = 0$ gives an exponential function that describes large particles with D larger than 200 μm, $\beta = 1$ gives a gamma distribution suitable in the range 20 - 200 μm, and $\beta = 2$ might apply to smaller particles with Do around 3-5 μm.

The reflectivity is given by

$$Ze = \int_0^{\infty} N(D) D^6 dD$$

$$Ze = A(\beta + 6)! / b^{(\beta + 7)}$$

The water content is thus related to the distribution by

$$WC = \pi \rho A(\beta + 3)! / [6\, b\, (\beta + 4)]$$

where ρ is the density.

We follow the conventional approach, using Ze, the water equivalent radar reflectivity factor.

The inference of cloud water content from radar measured reflectivities is a difficult task inasmuch as the relationship between Ze and LWC or IWC is not uniquely defined. In the past, numerous relationships have been proposed, which might not be applicable to clouds in more than one geographical area. The variability of

such a relationship is linked to the phase of the cloud particles, their density, and the particle size distribution (*Atlas et al.*, 1995; *Matrosov*, 1997).

To see what might be possible in terms of model validation, the cloud water profiles produced by the ECMWF model have been used with relationships in Table 8, linking the radar reflectivity at 35GHz with the cloud liquid or ice water content. For liquid water clouds, there is a reasonable agreement between relationships proposed by various authors to link Ze to LWC. Figure A1 (top) compares the relationships by *Atlas* (1954), *Sauvageot and Omar* (1987) and *Frisch et al.* (1995) to the one discussed by *Liao and Sassen* (1994). All the curves have a slope relatively close to unity, and the spread at both ends of the range (corresponding to LWC of $2x10^{-6}$ and 3.6 $g.m^{-3}$, respectively) is smaller than 2dBZ. Thus we can have confidence in inferences drawn for water clouds.

The situation for ice is far less clear, as various authors have shown from theoretical studies and/or observations, the relationship between Ze and IWC to be more variable for ice than for liquid water. *Atlas et al.* (1995) have shown IWC-Ze to depend on Do, the equivalent diameter, and on ΔDo, the spread around this diameter, using data from Kwajalein and FIRE-I. *Matrosov* (1997) discussed the variability of both IWC-Ze and Do-Ze from measurements taken during FIRE-II, ASTEX and the Arizona Program. *Brown et al.* (1995) also discussed related questions using 94 GHz-radar measurements during EUCREX and CEPEX. Using the model ice cloud content, Figure A1 (bottom) compares the reflectivities obtained with the IWC-Ze relationship of *Liao and Sassen* (1994) and those from *Atlas et al.* (1995), *Matrosov* (1997), and *Hogan and Illingworth* (1999).

When simulating the reflectivities from the model fields, we use the relationship from *Frisch et al.* (1995) for liquid water clouds assuming a droplet concentration N_0 of 900 cm^{-1}, and that from *Atlas et al.* (1995) assuming an equivalent diameter of Do of 100 μm. For simulating the reflectivity of the liquid water clouds, the chosen value of N_0 is consistent with what could be used if the effective radius were to be diagnosed for liquid water clouds (see section 4.3). Similarly, the 100 μm effective diameter for ice cloud particles is consistent with the effective radius (variable between 30 and 60 μm) used for computing the cloud optical properties in the radiation schemes.

In conclusion, the comparison of model and observed cloud reflectivities done in section 3.4 should allow an unambiguous validation of the model liquid water clouds from the radar data, but a far more uncertain validation of the model ice clouds.

ACKNOWLEDGMENTS

Dr. Clothiaux is gratefully thanked for providing the radar and micropulse lidar measurements used in this study. Thanks to Robin Perez for help in acquiring all the other observational data and pointing to the relevant documentation. These observational data were obtained from the Atmospheric Radiation Measurement (ARM) Program sponsored by the U.S. Department of Energy, Office of Science, Office of Biological and Environmental Research, Environmental Sciences Division. At ECMWF, Dominique Lucas is thanked for answering numerous queries about the HDF and NETCDF packages, Peter Bauer for help in making sense of the computation of radar reflectivity from the model cloud water, and Drs Hollingsworth, Miller, Beljaars, and Chevallier for their remarks on the manuscript.

REFERENCES

Atlas, D., 1954: The estimation of cloud parameters by radar. *J. Meteor.*, **11**, 309-317.

Atlas, D., S.Y. Matrosov, A.J. Heymsfield, M.-D. Chou, and D.B. Wolff, 1995: Radar and radiation properties of ice clouds. *J. Appl. Meteor.*, **34**, 2329-2345.

Beesley, J.A., C.S. Bretherton, C. Jakob, E.L. Andreas, J.M. Intrieri, and T.A. Uttal, 2000: A comparison of cloud and boundary layer variables in the ECMWF forecast model with observations at the Surface Heat Budget of the Arctic ocean (SHEBA) ice camp. *J. Geophys. Res.*, **105D**, 12337-12350.

Brown, P.R.A., A.J. Illingworth, A.J. Heymsfield. G.M. McFarquhar, K.A. Browning, and M. Gosset, 1995: The role of spaceborne millimeter-wave radar in the global monitoring of ice cloud. *J. Appl. Meteor.*, **34**, 2346-2366.

Clothiaux, E.E., T.P. Ackerman, G.C. Mace, K.P. Moran, R.T. Marchand, M.A. Miller, and B.E. Martner, 2000: Objective determination of cloud heights and radar reflectivities using a combination of active remote sensors at the ARM CART sites. *J. Appl. Meteor.*, **39**, 645-665.

Clothiaux, E.E., M.A. Miller, B.A. Albrecht, T.P. Ackerman, J. Verlinde, D.M. Babb, R.M. Peters, and W.J. Syrett, 1995: An evaluation of a 94-GHz radar for remote sensing of cloud properties. *J. Atmos. Oceanic Technol.*, **12**, 201-229.

Clothiaux, E.E., K.P. Moran, B.E. Martner, T.P. Ackerman, G.G. Mace, T. Uttal, J.H. Mather, K.B. Widener, M.A. Miller, and D.J. Rodriguez, 1999: The Atmospheric Radiation Measurement program cloud radars: Operational modes. *J. Atmos. Oceanic Technol.*, **16**, 819-827.

Darnell, W.L., W.F. Staylor, S.K. Gupta, N.A. Ritchey, and A.C. Wilber, 1992: Seasonal variation of surface radiation budget derived from ISCCP-C1 data. *J. Geophys. Res.*, **97D**, 15741-15760.

Dong, X., P. Minnis, T.P. Ackerman, E.E. Clothiaux, G.G. Mace, C.N. Long, and J.C. Liljegren, 2000: A 25-month database of stratus cloud properties generated from ground-based measurements at the ARM South Great Plains site. *J. Geophys. Res.*, **105D**, 4529-4538.

Ebert, E.E., and J.A. Curry, 1992: A parameterization of ice optical properties for climate models. *J. Geophys. Res.*, **97D**, 3831-3836.

Fouquart, Y., 1987: Radiative transfer in climate models. *NATO Advanced Study Institute on Physically-Based Modelling and Simulation of Climate and Climatic Changes*. Erice, Sicily, 11-23 May 1986. M.E. Schlesinger, Ed., Kluwer Academic Publishers, 223-284.

Fouquart, Y., and B. Bonnel, 1980: Computations of solar heating of the earth's atmosphere: a new parameterization. *Beitr. Phys. Atmosph.*, **53**, 35-62.

Frisch, A.S., C.W. Fairall, and J.B. Snider, 1995: Measurement of stratus cloud and drizzle parameters in ASTEX with a Ka-band Doppler radar and a microwave radiometer. *J. Atmos. Sci.*, **52**, 2788-2799.

Fu, Q., 1996: An accurate parameterization of the solar radiative properties of cirrus clouds for climate studies. *J. Climate*, **9**, 2058-2082.

Fu, Q., and K.-N. Liou, 1993: Parameterization of the radiative properties of cirrus clouds. *J. Atmos. Sci.*, **50**, 2008-2025.

Fu, Q., P. Yang, and W.B. Sun, 1998: An accurate parameterization of the infrared radiative properties of cirrus clouds of climate models. *J. Climate*, **11**, 2223-2237.

Garratt, J.R., 1994: Incoming shortwave fluxes at the surface: A comparison of GCM results with observations. *J. Climate*, **7**, 72-80.

Garratt, J.R., A.J. Prata, 1996: Downwelling longwave fluxes at continental surfaces - A comparison of observations with GCM simulations and implications for the global land-surface radiation budget. *J. Climate*, **9**, 646-655.

Garratt, J.R., A.J. Prata, L.D. Rotstayn, B.J. McAvaney, and S. Cusack, 1998: The surface radiation budget over oceans and continents. *J. Climate*, **11**, 1951-1968.

Gibson, J.K., P., Kallberg, S. Uppala, A. Nomura, A. Hernandez, and E. Serrano, 1997: The ECMWF Re-Analysis description. *ECMWF Re-Analysis Project Report Series*, Vol 1.

Gregory, D., J.-J. Morcrette, C. Jakob, A.C.M. Beljaars, and T. Stockdale, 2000 : Revision of convection, radiation and cloud schemes in the ECMWF Integrated Forecasting System. *Quart. J. Roy. Meteor. Soc.*, **126**, 1685-1710.

Hogan, R.J., and A.J. Illingworth, 1999: The potential of spaceborn dual-wavelength radar to make global measurements of cirrus clouds. *J. Atmos. Ocean. Technol.*, **16**, 518-531.

Holloway, J.L., and S. Manabe, 1971: Simulation of climate by a global general circulation model. 1. Hydrologic cycle and heat balance. *Mon. Wea. Rev.*, **99**, 335-370.

Hortal, M., and A.J. Simmons, 1991: Use of reduced Gaussian grids in spectral models. *Mon. Wea. Rev.*, **119**, 1057-1074.

Hortal, M., 2000: The development and testing of a new two-time-level semi-Lagrangian scheme (SETTLS) in the ECMWF forecast model. *Quart. J. Roy. Meter. Soc.*, in press.

Illari, L., 1987: The "spin-up" problem. *ECMWF Research Dept. Tech. Memo.* No. 137, 31 pp., ECMWF, Reading, U.K.

Jakob, C., and S.A. Klein, 2000: A parametrization of the effects of cloud and precipitation overlap for use in general circulation models. *Quart. J. Roy. Meteor. Soc.*, **126C**, 2525-2544.

Kosarev, A.L., and I.P. Mazin, 1991: An empirical model of the physical structure of upper-level clouds. *Atmos. Res.*, **26**, 213-228.

Laszlo, I., and R.T. Pinker, 1993: Shortwave cloud-radiative forcing at the top of the atmosphere, at the surface and of the atmospheric column as determined from ISCCP C1 data. *J. Geophys.Res.*, **98D**, 2703-2718.

Li, Zhanqing, and H.G. Leighton, 1993: Global climatologies of solar radiation budgets at the surface and in the atmosphere from 5 years of ERBE data. *J. Geophys. Res.*, **98D**, 4919-4930.

Liao, L., and K. Sassen, 1994: Investigation of relationships between Ka-band radar reflectivity and ice and liquid water contents. *Atmosph. Research*, **34**, 231-248.

Mace, G.G., C. Jakob, and K. P. Moran, 1998: Validation of hydrometeor occurrence predicted by the ECMWF model using millimeter wave radar data. *Geophys. Res. Letters*, **25**, 1645-1648.

Mahfouf, J.-F., and F. Rabier, 2000: The ECMWF operational implementation of four dimensional variational assimilation: Part II: Experimental results with improved physics. *Quart. J. Roy. Meteor. Soc.*, **126A**, 1171-1190.

Martin, G.M., D.W. Johnson, and A. Spice, 1994: The measurement and parameterization of effective radius of droplets in warm stratocumulus. *J. Atmos. Sci.*, **51**, 1823-1842.

Matrosov, S.Y., 1997: Variability of microphysical parameters in high-altitude ice clouds: Results of the remote sensing methods. *J. Appl. Meteor.*, **36**, 633-648.

Matveev, Yu. L., 1984 : Cloud dynamics. D. Reidel Publishing Co., Dordrecht, 340 pp.

Miller, S.D., G.L. Stephens, and A.C.M. Beljaars, 1999: A validation survey of the ECMWF prognostic cloud scheme using LITE. *Geophys. Res. Letters*, **26**, 1417-1420.

Mlawer, E.J., S.J. Taubman, P.D. Brown, M.J. Iacono, and S.A. Clough, 1997: Radiative transfer for inhomogeneous atmospheres: RRTM, a validated correlated-k model for the longwave. *J. Geophys. Res.*, **102D**, 16,663-16,682.

Morcrette, J.-J., 1991: Radiation and cloud radiative properties in the ECMWF operational weather forecast model. *J. Geophys. Res.*, **96D**, 9121-9132.

Morcrette, J.-J., 1993: Revision of the clear-sky and cloud radiative properties in the ECMWF model. *ECMWF Newsletter*, **61**, 3-14.

Morcrette, J.-J., S.A. Clough, E.J. Mlawer, and M.J. Iacono, 1998: Impact of a validated radiative transfer scheme, RRTM, on the ECMWF model climate and 10-day forecasts. *ECMWF Technical Memo.* No. 252, 47 pp.

Morcrette, J.-J., 2000: On the effects of the temporal and spatial sampling of radiation fields on the ECMWF forecasts and analyses. *Mon. Wea. Rev.*, **128**, 876-887.

Ohmura, A., and H. Gilgen, 1993: Re-evaluation of the global energy balance. in "Interactions between Global Climate Subsystems", *Amer. Geophys. Union, Geophys. Monogr.*, **75**, 15, 93-110.

Rabier, F., J.-N. Thepaut, and P. Courtier, 1998: Extended assimilation and forecasts experiments with a four dimensional variational assimilation system. *Quart. J. Roy. Meteor. Soc.*, **124**, 1861-1887.

Sassen, K., 1987: Ice cloud content from radar reflectivity. *J. Climate Appl. Meteorol.*, **26**, 1050-1053.

Sauvageot, H., and J. Omar, 1987: Radar reflectivity of cumulus clouds. *J. Atmos. Oceanic Technol.*, **4**, 264-272.

Wild, M., A. Ohmura, H. Gilgen, J.-J. Morcrette, and A. Slingo, 2000: Evaluation of the downward longwave radiation in general circulation models. *J. Climate*, accepted.

Wild, M., A. Ohmura, H. Gilgen, J.-J. Morcrette, and A. Slingo, 2000: Evaluation of the downward longwave radiation in general circulation models. *J. Climate*, accepted.

Observational System	Acronym	Observed/Retrieved Physical Quantities	Original Data Frequency
Atmospheric Emitted Radiance Interferometer	AERI	Planetary Boundary Layer temperature and water vapour profiles	~ 480 s
Belfort Laser Ceilometer	BLC	Base height of lowest cloud	30 s
Energy Balance Bowen Ratio	EBBR	Air temperature and relative humidity, soil temperature, net radiation, surface pressure	1800 s
GOES-8	GOES8	Radiances at 3.9, 6.9, 10.9 and 11.6 μm Retrieved T and Td	30 mn to 2 hours
Micropulse Lidar	MPL	Cloud boundaries	~ 60 s
Multi-Mode Cloud Radar	MMCR	Cloud boundaries, mask and reflectivity	10 s
Microwave Radiometer	MWR	Cloud integrated amounts of water vapour and cloud liquid water	20 s
Solar Infrared Radiation Stations	SIRS	Up- and downwelling longwave and shortwave radiation	60 s
Sonde	SONDE	temperature and dew point profiles	2 to 4 daily
Surface Meteorological Observation System	SMOS	Air temperature and relative humidity, surface pressure, precipitation	1800 s

Table 1: Observational data used in this study: Central Facility

	Unit	000-024		006-030		012-036	
Surf. Pressure	hPa	975.2	(7.0)	975.1	(7.0)	975.1	(6.9)
Skin Temperature	K	291.7	(6.5)	291.8	(6.6)	291.7	(6.6)
Surf. Albedo	Percent	14.76	(0.002)	14.76	(0.002)	14.76	(0.002)
Total Cloud Cover	Percent	38.9	(0.4)	38.8	(0.4)	40.4	(0.4)
Low Level Cloudiness	Percent	15.2	(0.3)	14.2	(0.3)	14.9	(0.3)
Column Water vapour	kg m^{-2}	21.7	(10.0)	21.9	(10.2)	22.2	(10.3)
Column Cloud Water	g m^{-2}	162	(11)	168	(12)	185	(13)
Soil Moisture	mm	292	(35)	291	(35)	292	(36)
Downward SW Flux	W m^{-2}	258.1	(329.6)	260.0	(331.3)	259.2	(333.0)
Downward LW Flux	W m^{-2}	339.8	(46.1)	339.6	(46.1)	339.4	(45.8)
Latent Heat Flux	W m^{-2}	119.6	(137.6)	121.3	(139.3)	121.9	(141.3)
Sensible Heat Flux	W m^{-2}	21.1	(95.0)	20.6	(94.3)	20.5	(94.6)
ToA Net SW Flux	W m^{-2}	320.4	(371.9)	321.9	(373.2)	321.5	(374.2)
ToA Outgoing LW Flux	W m^{-2}	260.3	(29.6)	259.6	(29.8)	258.3	(30.5)

Table 2: Comparison of model quantities for different ranges within the forecasts over the April-May 1999 period.

Values are the time-averages of the various parameters, and between brackets, the corresponding standard deviation.

	Nobs	C1	E13	correlation	slope	intercept
Surface Pressure	979	974.6 (6.4)	975.3 (6.4)	0.998	0.995	5.5
Skin Temperature	979	291.0 (6.8)	291.4 (7.0)	0.989	1.021	-5.6
TCWV	142	20.3 (8.3)	18.6 (7.9)	0.985	0.937	-0.3
Downward SW	1068 1069 603	249.4 (329.9) 251.4 (328.2) 445.6 (323.1)	247.9 (329.6) 250.4 (327.4 443.8 (322.8)	1.000 1.000 1.000	0.999 0.998 0.999	-1.2 -0.5 -1.4
Downward LW	1075	337.6 (47.4)	340.7 (47.1)	0.999	0.993	5.6

Table 3: Statistics of measurements at two neighbouring locations over the April-May period.

TCWV is the vertically integrated water vapour (total column water vapour, in kg m^{-2}). Statistics for the surface downward SW radiation are given averaged over all measurements, averaged over all measurements setting the (slightly negative) nighttime values to zero (see text), and averaged over daytime only.

	Nobs	Model	CF Obs.	correlation	slope	intercept
clear-sky conditions						
TCWV	168	12.06 (5.48)	12.51 (5.41)	0.986	0.999	-0.15
Downward LW	168	292.2 (34.1)	294.1 (33.7)	0.993	1.006	-3.6
Downward SW	164	601.5 (337.5)	570.3 (321.5)	0.998	1.048	3.7
overcast conditions						
TCWV	59	27.73 (8.42)	26.95 (9.29)	0.925	0.838	5.13
Downward LW	59	359.3 (41.8)	357.5 (41.0)	0.985	1.005	0.0
Downward SW	25	96.3 (108.8)	69.9 (102.8)	0.916	0.963	29.9
all conditions						
Downward LW	1436	339.4 (46.1)	341.3 (44.0)	0.899	0.942	17.8
Downward SW	821	430.0 (323.6)	412.9 (321.6)	0.917	0.923	48.9

Table 4: Statistics of comparisons between model and observations in April-May 1999.

Clear-sky and overcast conditions are assumed when the model and observed total cloudiness are < 1% and > 99%, respectively.

	SDLWC	SDLWT	SDSWC	SDSWT
RRTM / SW4 aerosols	307.1	322.4	307.7 571.0	245.4 455.4
RRTM / SW4 no aerosol	306.7	322.1	323.3 599.9	257.8 478.4
M91_LW / SW2 aerosols	301.8	317.1	307.5 570.6	244.5 453.7
M91_LW / SW2 no aerosol	301.5	316.8	322.9 599.2	256.8 476.4

Table 5: Impact of various model configurations on the monthly averaged surface radiation fluxes for April 1999.

SD indicates down fluxes at the surface. LW and SW are for longwave and shortwave fluxes respectively; C is for clear sky and T for total sky fluxes. All fluxes in W m^{-2}. For SDSWC and SDSWT, fluxes are given averaged over daytime periods only for the total two-month period. RRTM and M91 refer to the Rapid Radiation Transfer Model (*Mlawer et al.*, 1997) and *Morcrette* (1991) longwave radiation schemes; SW4 and SW2 refer to the shortwave scheme of *Morcrette* (1991) with either 4 or 2 spectral intervals.

	LW optical properties	SDLWT	SW optical properties	SDSWT
RRTM / SW4	SS92+EC92	323.4 338.3	YF87 + EC92	245.4 455.4 410.3
	SR97+EC92	323.3 338.2	AS89 + EC92	241.6 448.2 401.0
	SR97+FL93	323.4 338.4	AS89 + F96	244.6 453.9 408.3

Table 6: Impact of the cloud optical properties for April 1999 simulations

For liquid water clouds, the cloud optical properties are taken in the longwave either from *Smith and Shi* (1992), or *Savijarvi and Raisanen* (1997), in the shortwave either from *Fouquart* (1987) or *Slingo* (1989). For ice water clouds, the cloud optical properties are taken in the longwave either from *Ebert and Curry* (1992), or *Fu and Liou* (1993), in the shortwave either from *Ebert and Curry* (1992), or *Fu* (1996).

	Ntot	SDLWT	SDSWT
RRTM / SW4 SS92 + EC92	300	323.4 338.3	242.5 450.0 403.2
	600	338.4 338.3	240.0 445.3 397.1
	900	323.4 338.3	239.0 443.5 394.8
	1200	323.4 338.3	238.6 442.8 393.9

Table 7: Impact of the dimension of the water cloud effective radius for April 1999 simulations

For the surface downward shortwave total radiation, the three values correspond to the average over all 720 one-hour simulations in April 1999, to the average over the daytime cases, and to the average over the daytime cases for which the total cloudiness is larger than 1 percent.

References	Ice	Liquid
Atlas, 1954		$LWC = 4.56\ Ze^{0.5}$ $Z_e = 0.048\ LWC^2$
Sassen, 1987	$IWC = 0.037\ Z_e^{0.7}$ $Ze = 111.6\ IWC^{1.43}$	
Sauvageot and Omar, 1987		$LWC = 5.06\ Ze^{0.53}$ $Z_e = 0.047\ LWC^{1.83}$
Liao and Sassen, 1994	$IWC = 0.027\ Z_e^{0.78}$ $Z_e = 102.6\ IWC^{1.28}$	$LWC = 7.49\ Z_e^{0.78}$ $Z_e = 0.076\ LWC^{1.28}$
Atlas et al., 1995	$IWC = 0.064\ Z_e^{0.55}$ $Z_e = 148.0\ IWC^{1.82}$	
Frisch et al., 1995		$LWC = 0.30\ \rho_w\ Z^{0.5}\ N_0^{0.5}$
Matrosov, 1997	$IWC = 0.112\ Z_e^{0.68}$ $Z_e = 25\ IWC^{1.47}$ $IWC = 0.095\ Z_e^{0.48}$ $Z_e = 134.7\ IWC^{2.08}$	
Hogan and Illingworth, 1999	$\log_{10}(IWC)=0.0619Z_e-1.078$ $\log_{10}(IWC)=0.0617Z_e-0.899$	

Table 8: Relationship between 35GHz reflectivity and cloud water content

For *Matrosov* (1997), the sets of formulas correspond to two extreme cases (ASTEX 23 June 1992 and Arizona Program 3 March 1995) respectively showing a high and low correlation between reflectivity and IWC. For *Hogan and Illingworth* (1999), the sets of formulas correspond to ASTEX and CEPEX cases, respectively.

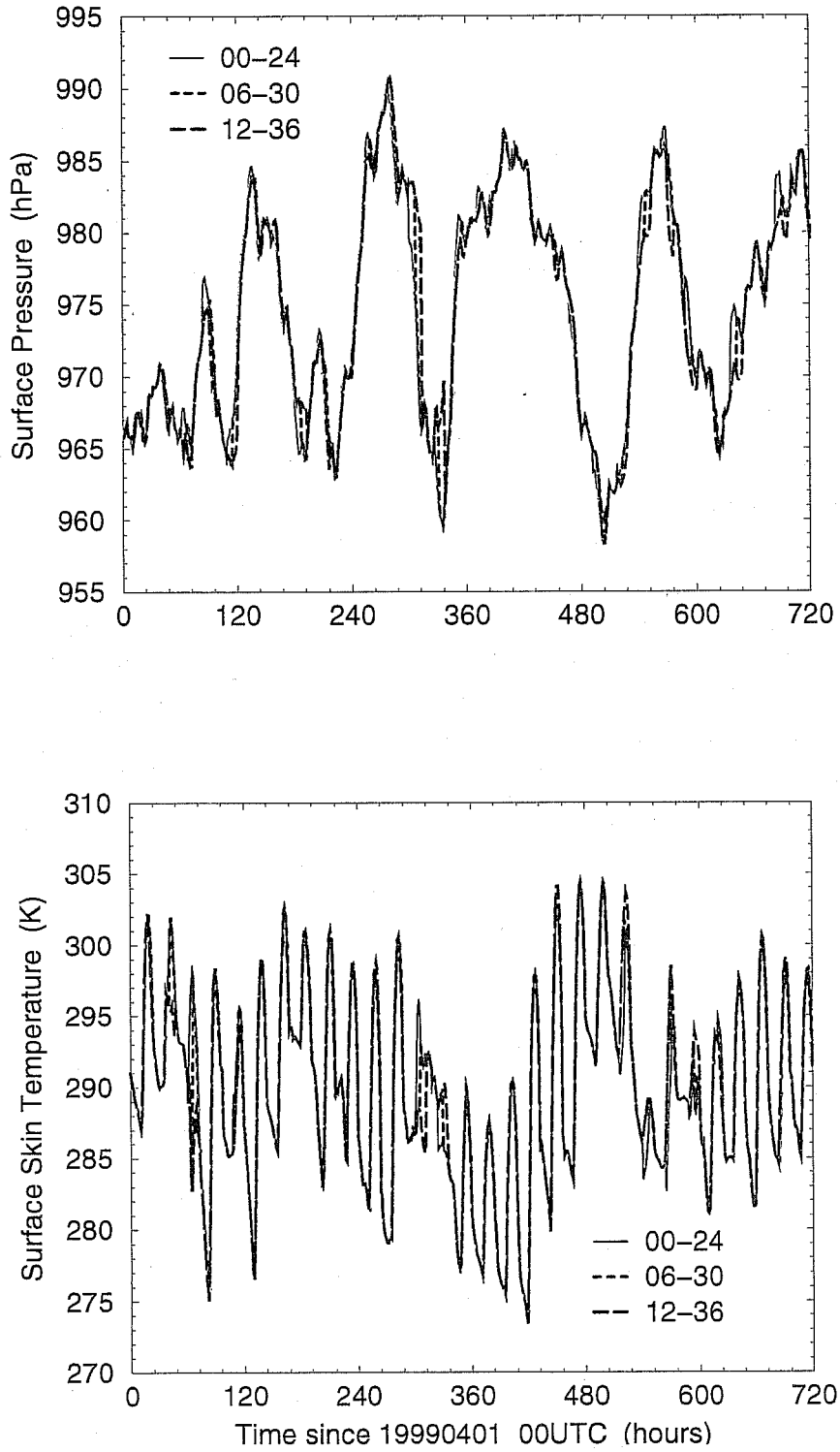

Figure 1a: The model surface pressure (top) and skin temperature (bottom) over the ARM-SGP site in April 1999, taken for various forecast times (00 to 24, 06 to 30 and 12 to 36 hours in the forecast).

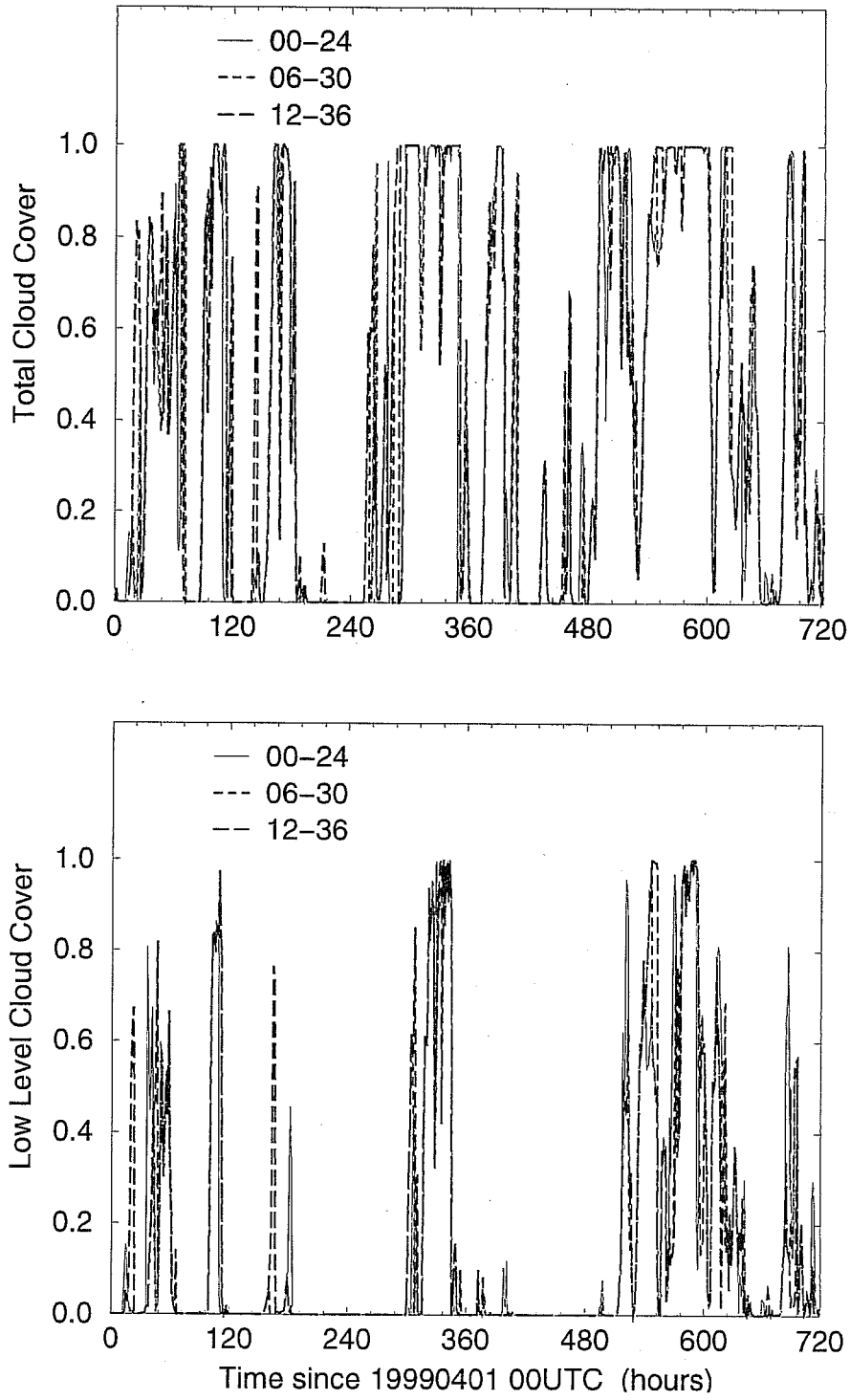

Figure 1b: The model total cloudiness (top) and low-level cloudiness (bottom) over the ARM-SGP site in April 1999, taken for various forecast times (00 to 24, 06 to 30 and 12 to 36 hours in the forecast).

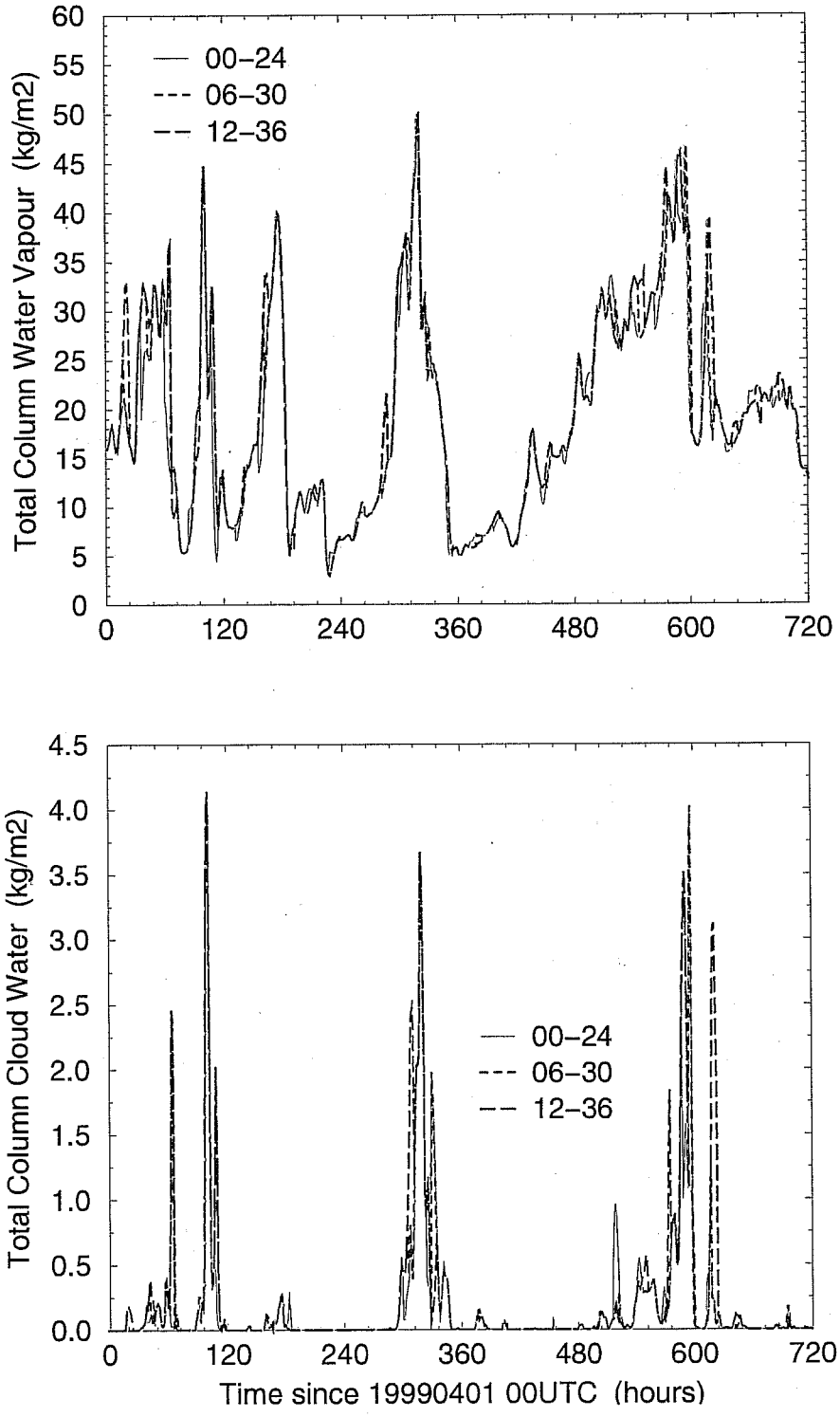

Figure 2a: As in Fig. 1, but for the vertically integrated water vapour (top) and vertically integrated cloud water.

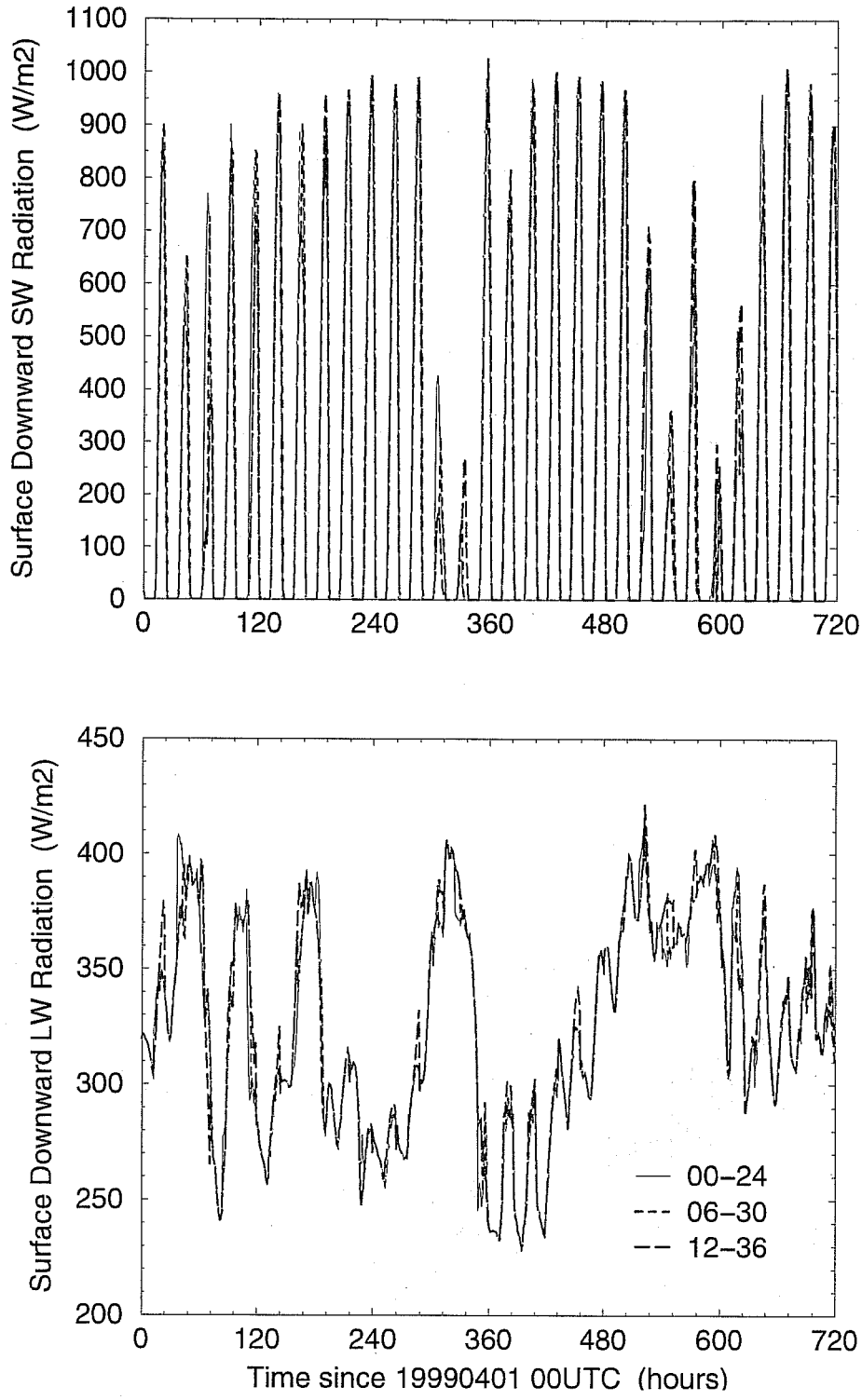

Figure 2b: As in Fig. 1, but for the surface downward shortwave (top) and downward longwave radiation (bottom).

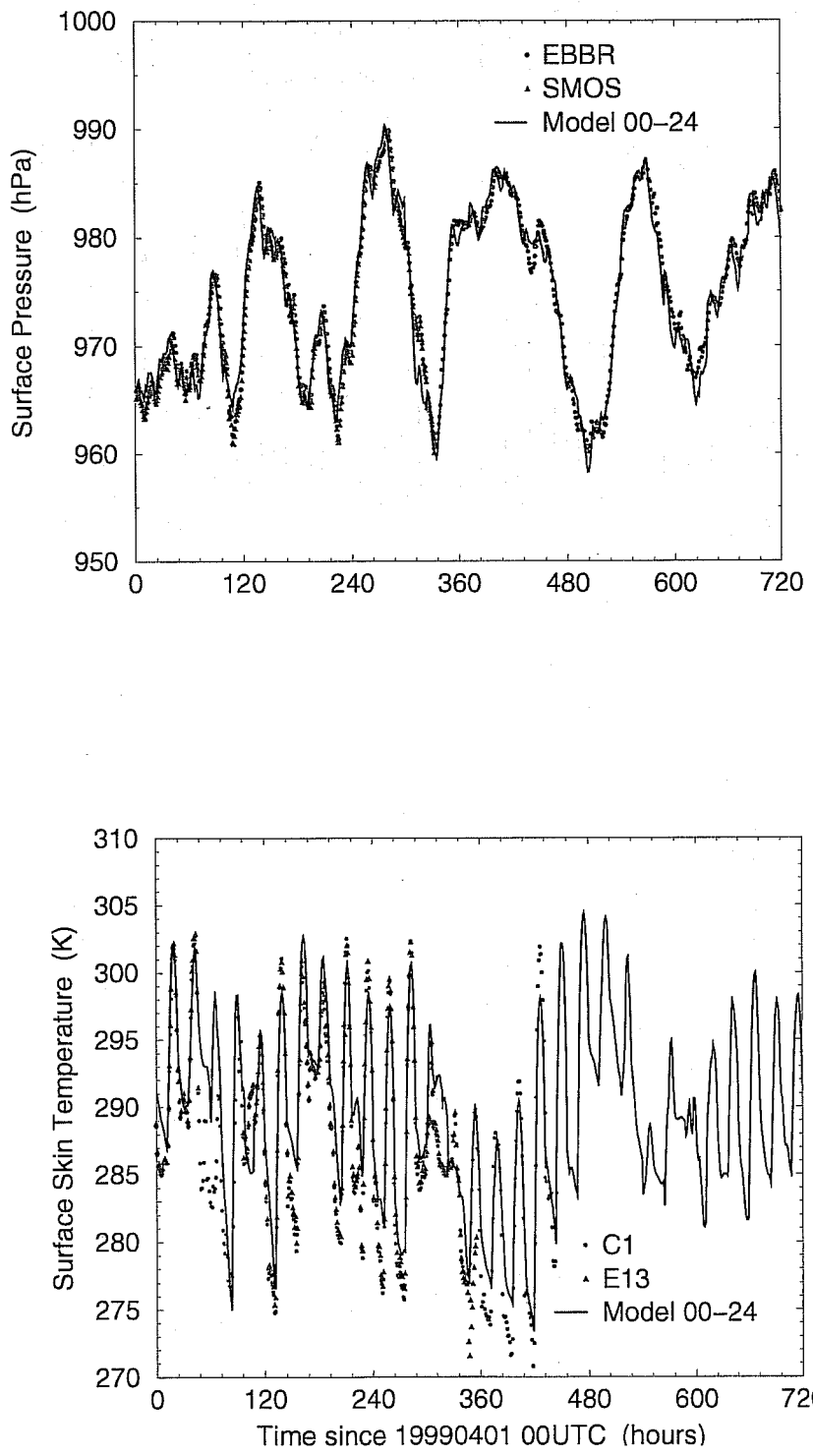

Figure 3: The surface pressure (top) and surface skin temperature (bottom) over the ARM-SGP Central Facility. Measurements are from the Energy Balance Bowen Ratio system and synoptic measurements for pressure, and derived from Solar Infrared Radiation stations C1 and E13 for skin temperature.

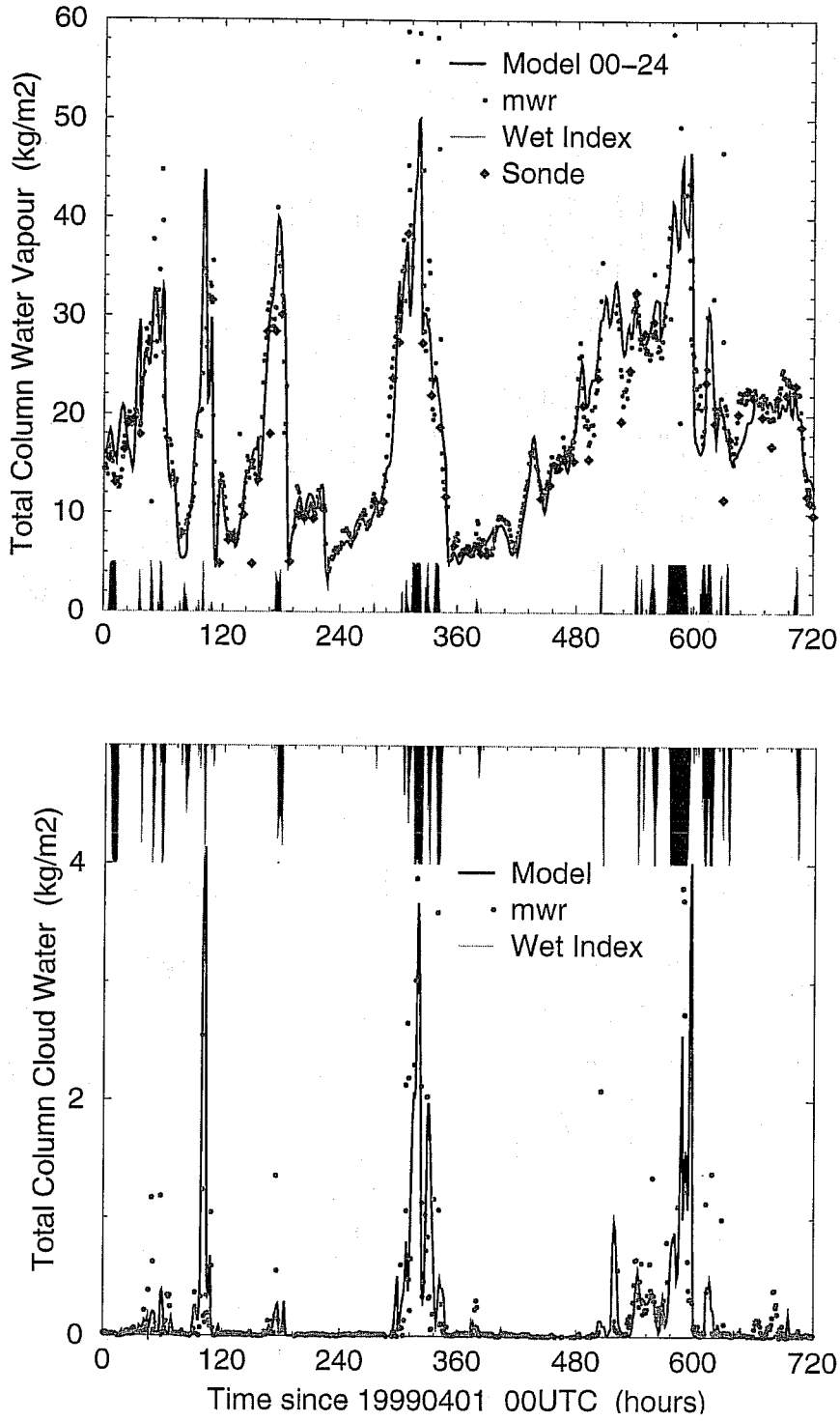

Figure 4: The vertically integrated water vapour (top) and vertically integrated cloud water (bottom) over the ARM-SGP Central Facility. Measurements are from the Microwave Radiometer.

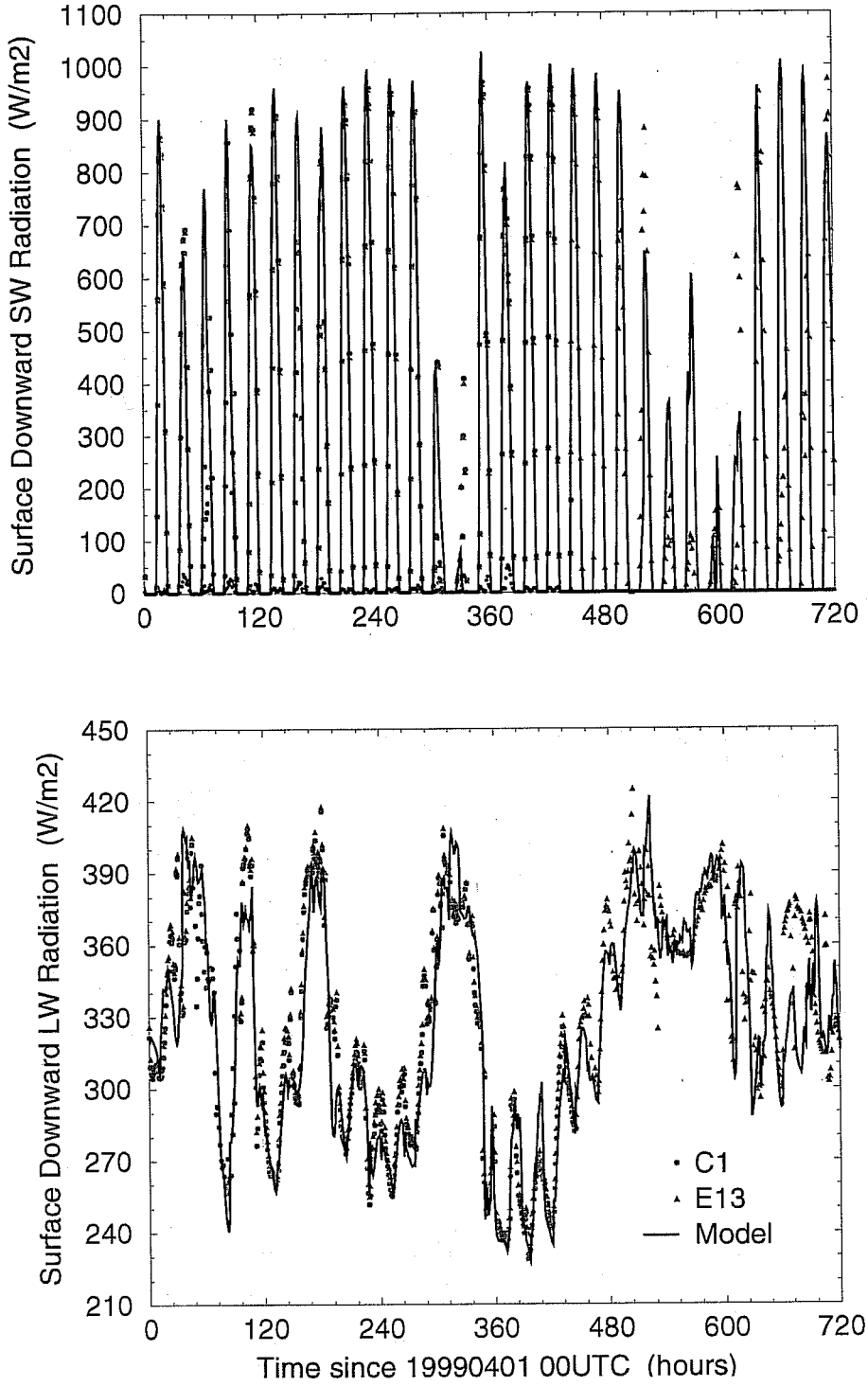

Figure 5: The surface downward shortwave (top) and longwave radiation (bottom) from the SIRS-C1 and E13 , and from the 00-24-hour model. Measurements are from Solar Infrared Radiation stations C1 and E13.

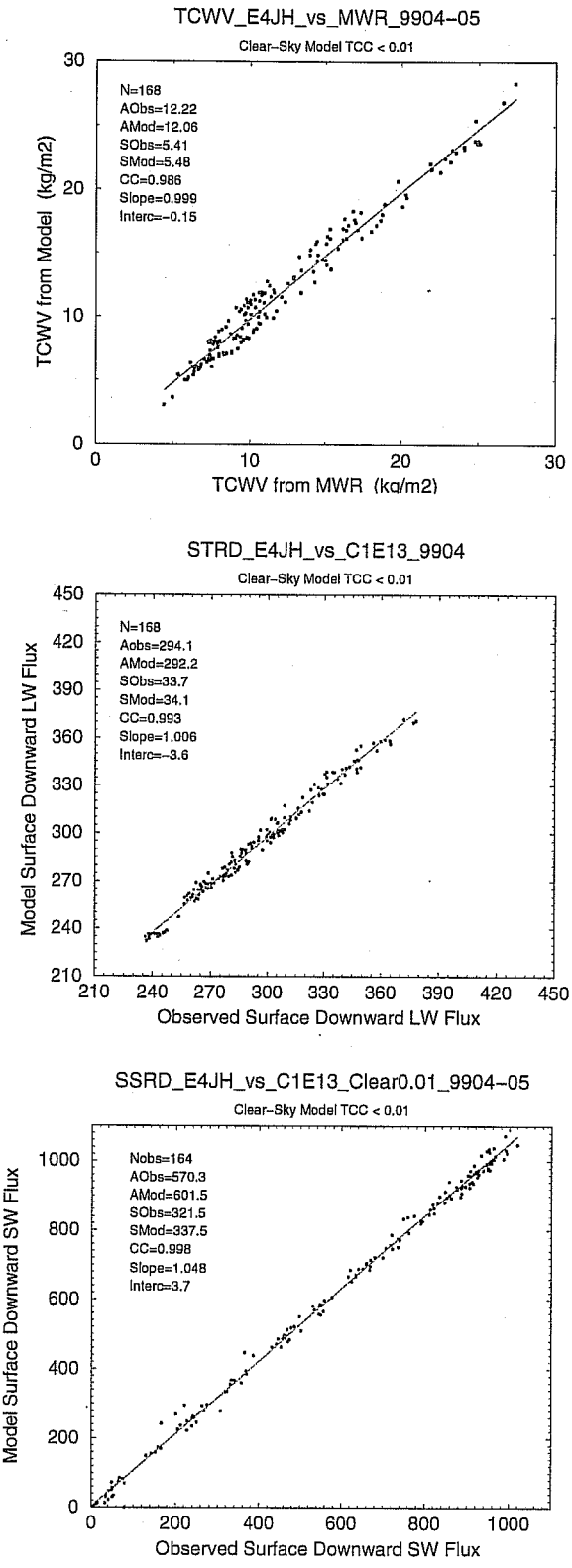

Figure 6: The total column water vapour (top panel), surface downward LW (middle panel)and SW radiation (bottom panel) for the set of clear-sky conditions.

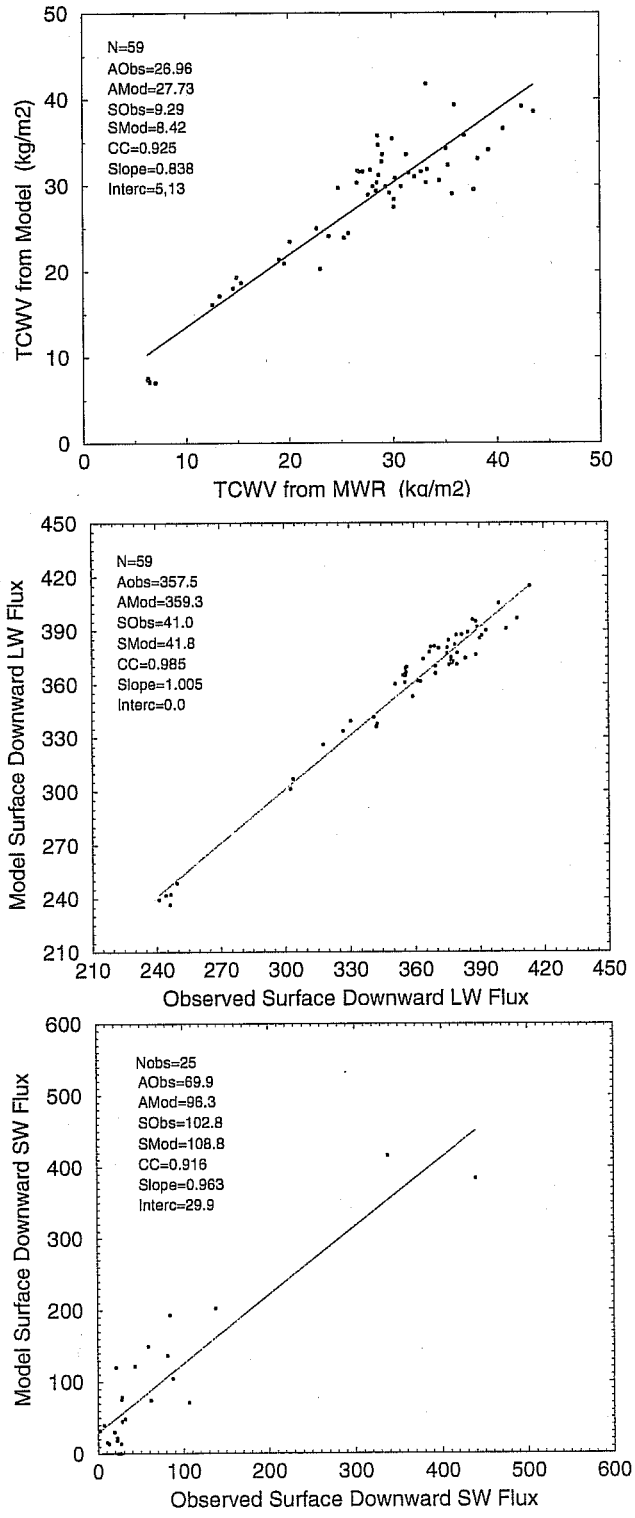

Figure 7: As in Fig. 6, but for the set of overcast sky conditions.

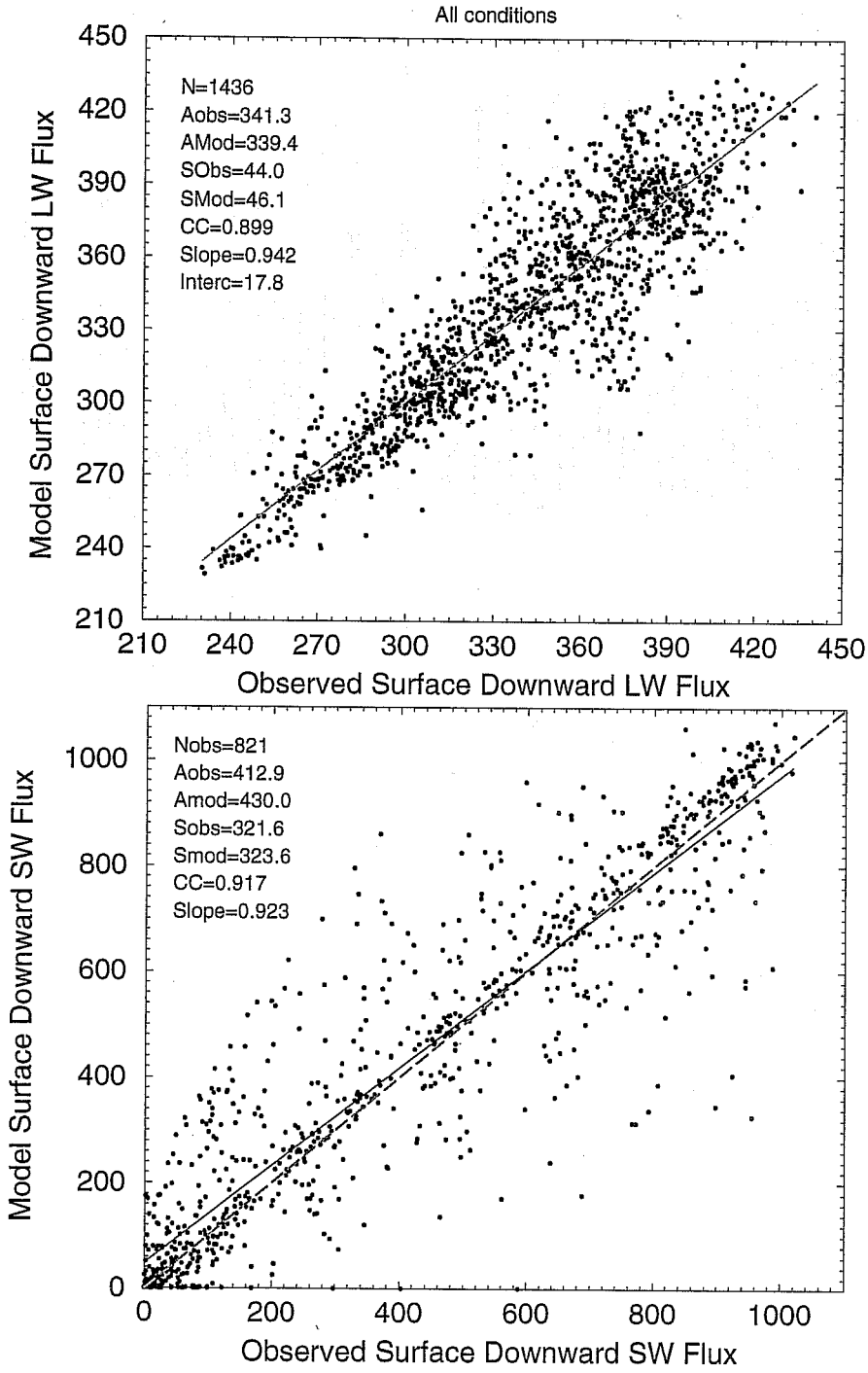

Figure 8: Comparison of the model and observed surface downward LW (top panel) and SW (bottom panel) radiation over all possible match-ups in April-May 1999.

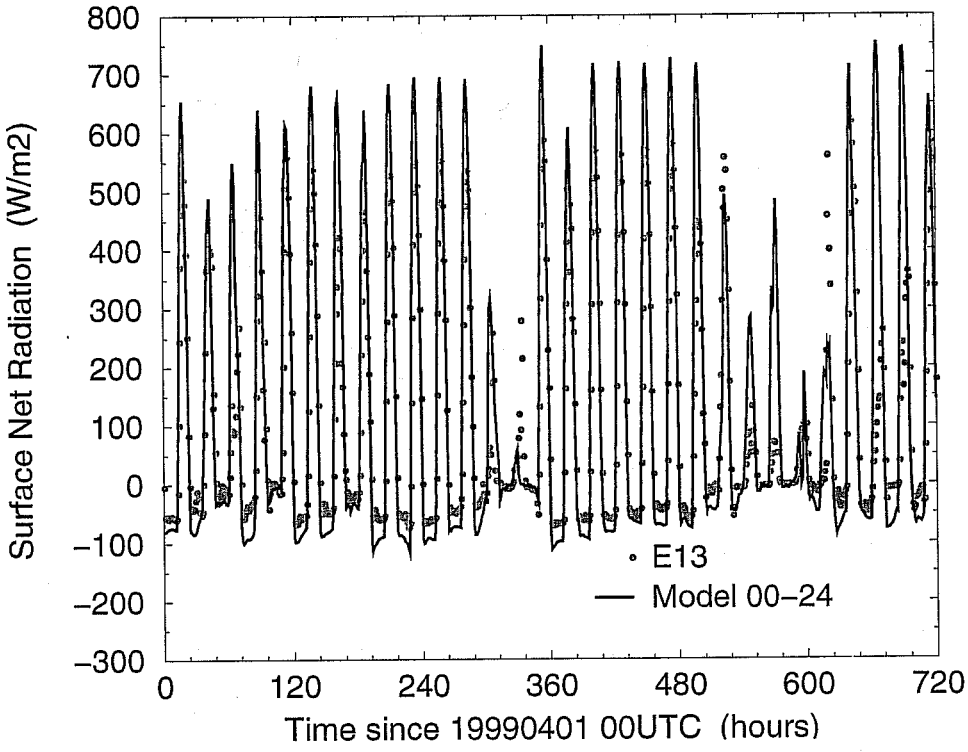

Figure 9: The surface net radiation from the EBBR- E13 station, and from the 00-24-hour model.

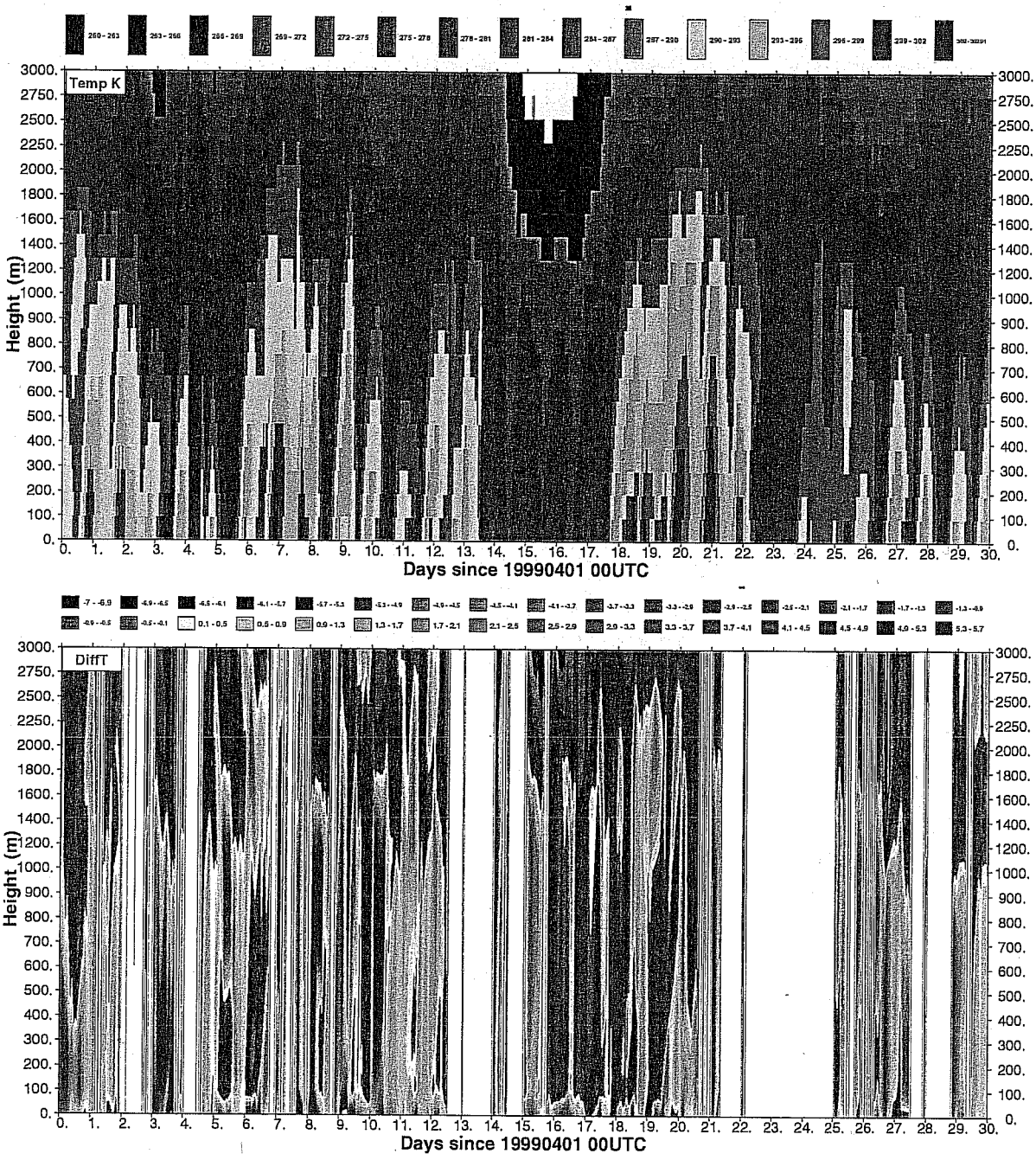

Figure 10: The temperature in the first 3000 m derived from the ECMWF model 00-24-hour forecasts (top panel). Step is 3 K, starting from 260 K. Bottom panel shows the difference between the model-simulated and the AER interferometer observation-derived temperature. For the differences, shading starts at +/- 0.1K with a 0.4K thereafter.

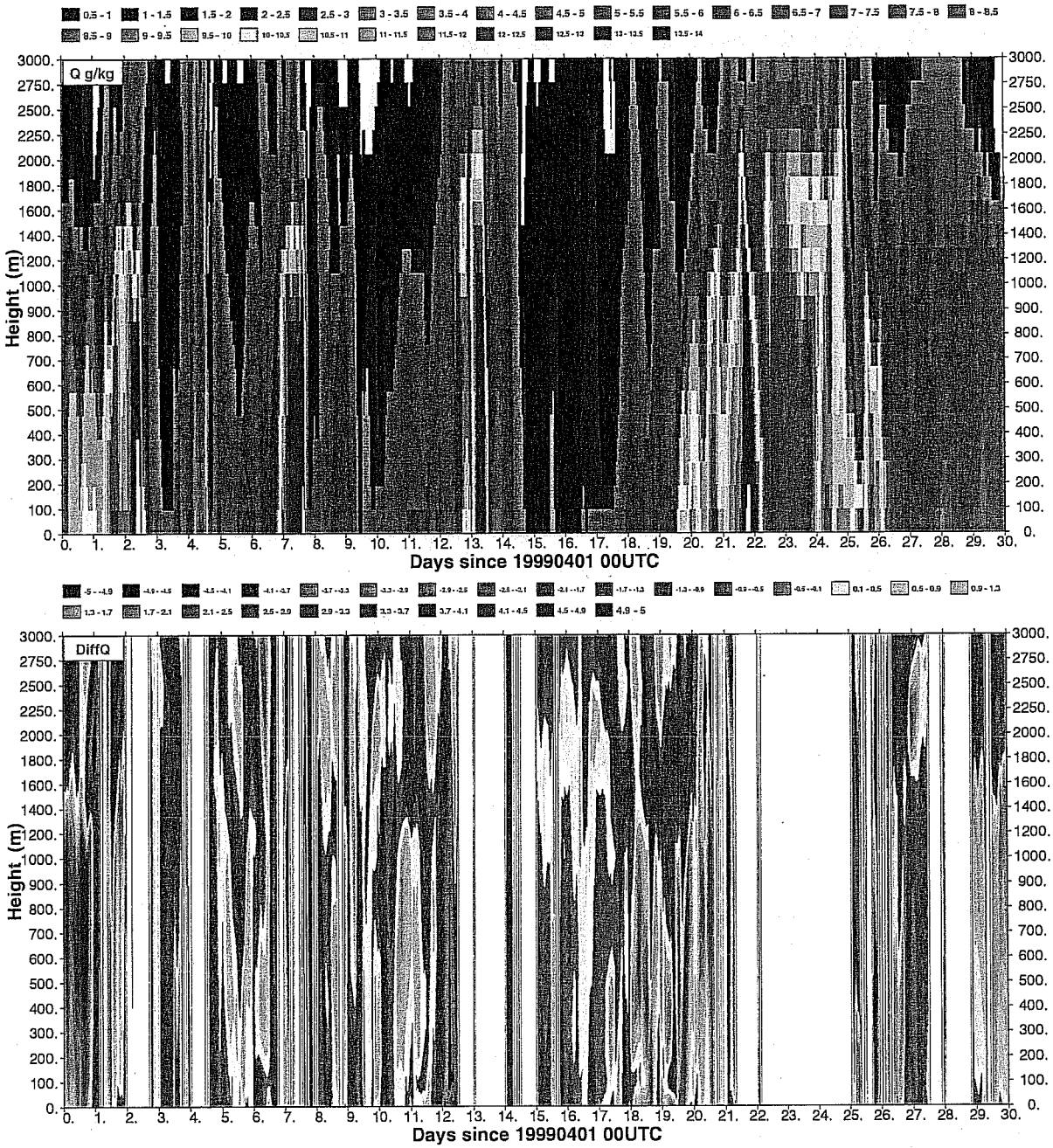

Figure 11: The humidity in the first 3000 m derived from the ECMWF model 00-24-hour forecasts (top panel). Step is 0.5 g/kg starting from 0.5 g/kg. Bottom panel shows the difference between the model-simulated and the AER interferometer observation-derived humidity. For the differences, shading starts at +/- 0.1g/kg with a 0.4g/kg thereafter.

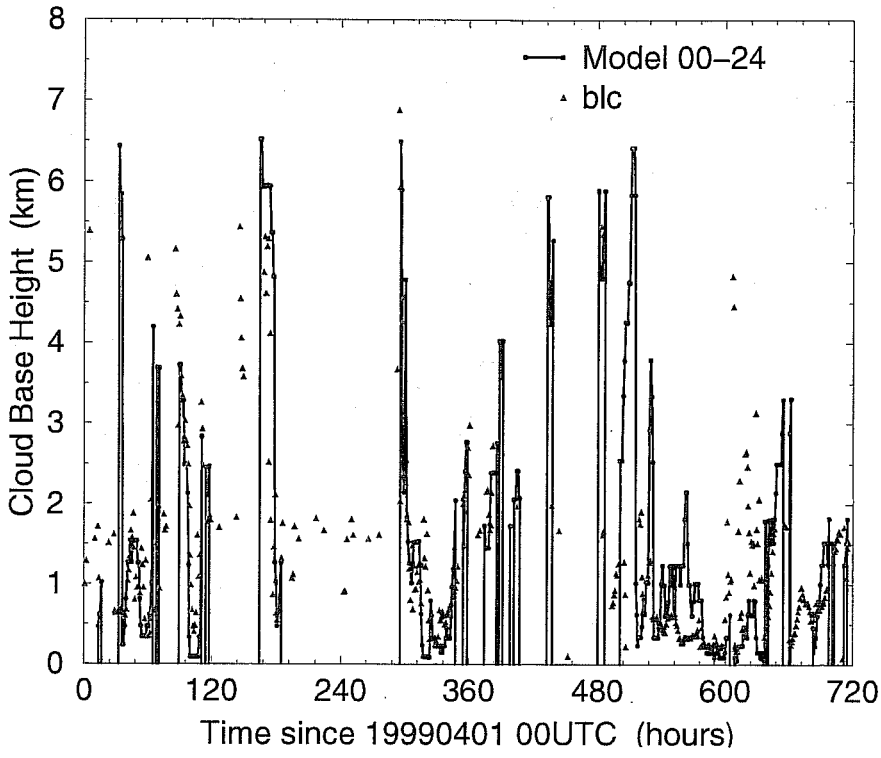

Figure 12: The cloud base height as produced by the model and measured by the Belfort Laser Ceilometer.

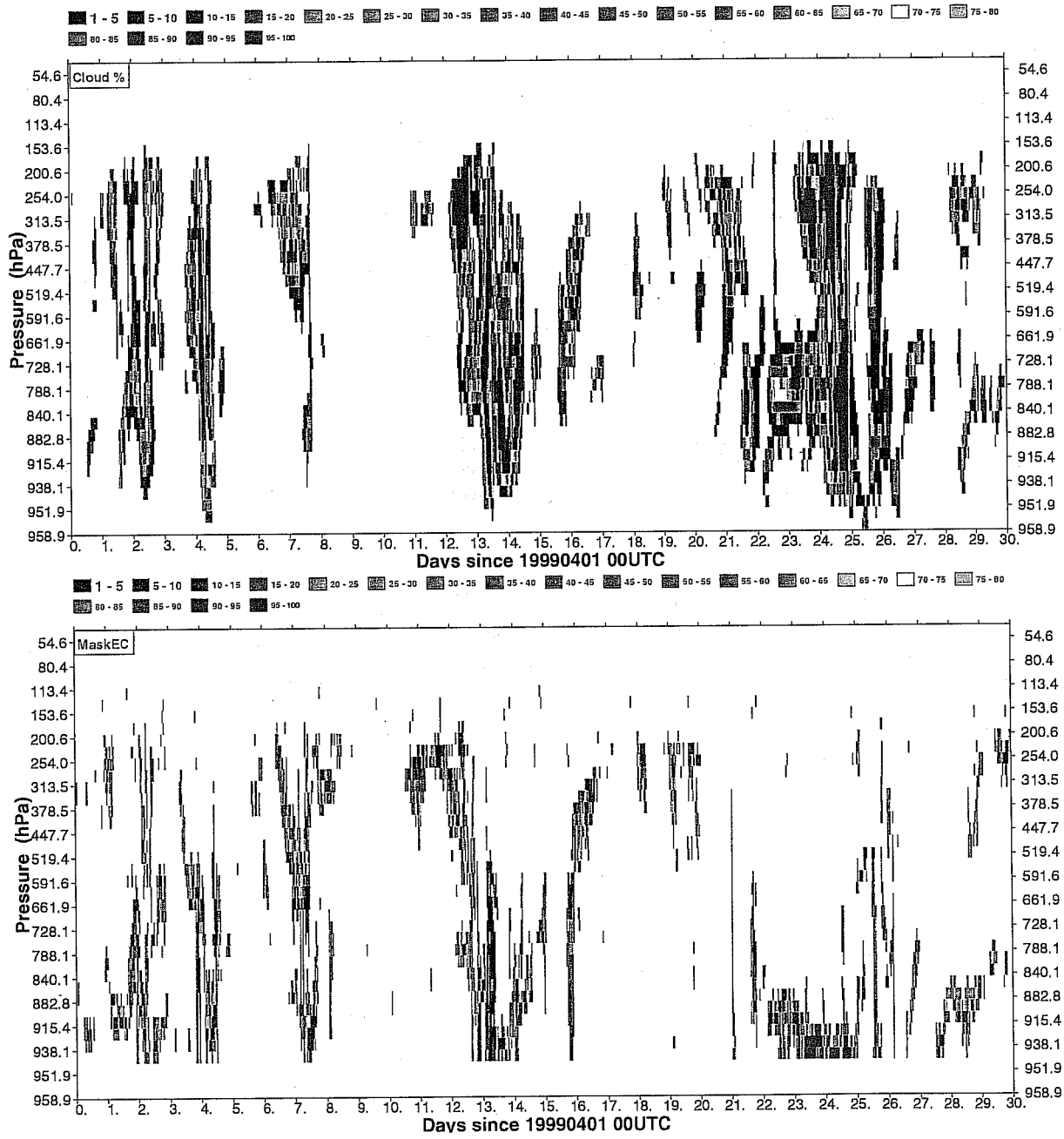

Figure 13: Time-series of the cloud cover (percent) from the series of ECMWF model 00-24hour forecasts (top panel) and the cloud mask derived from MMCR measurements using Clothiaux et al. (1995)'s algorithm (bottom panel). Step is 5 percent.

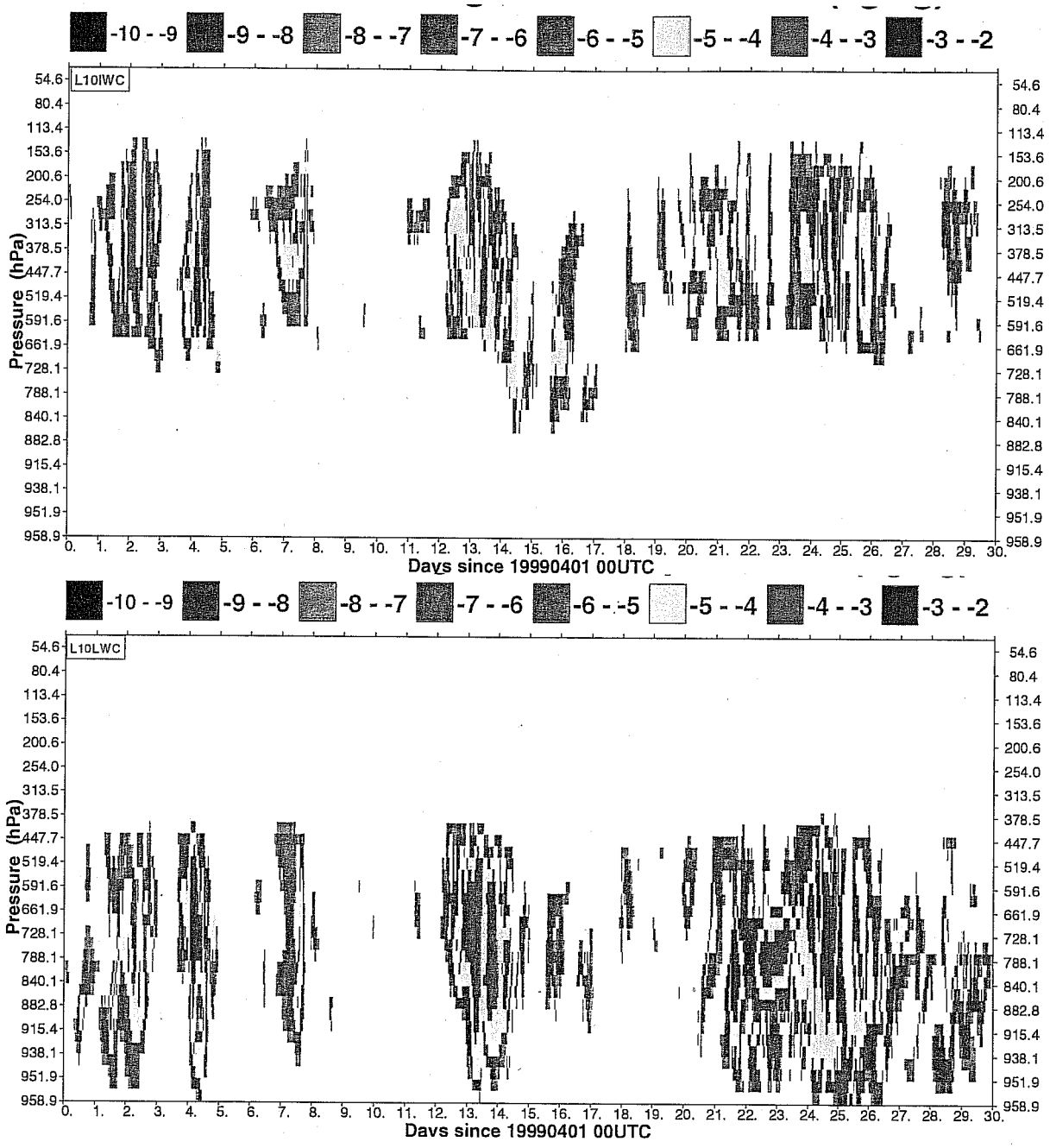

Figure 14: The cloud ice water (top panel) and cloud liquid water (bottom panel) produced by the ECMWF model over the ARM-SGP site (top panel). Plotted quantity is the decimal logarithm of the cloud water content in g m^{-3}.

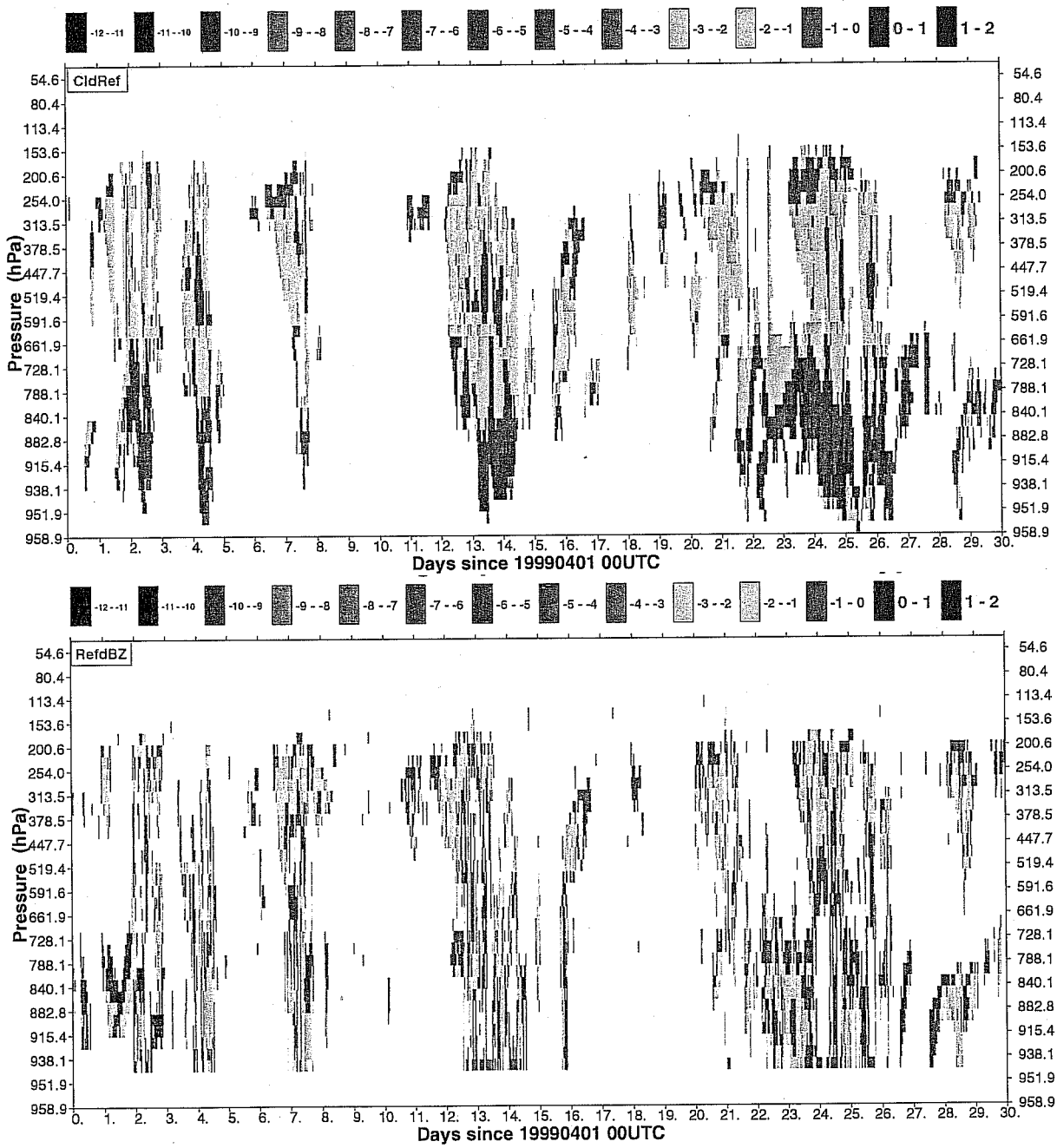

Figure 15: The pseudo-radar reflectivity computed from the ECMWF model using the relationships from Frisch et al. (1995) for LWC-Ze, and Atlas et al. (1995) for IWC-Ze (top panel) and the radar reflectivity actually measured at the ARM-SGP site. The reflectivity is the best estimate as discussed in Clothiaux et al. (2000). Step is 1 dBZ.

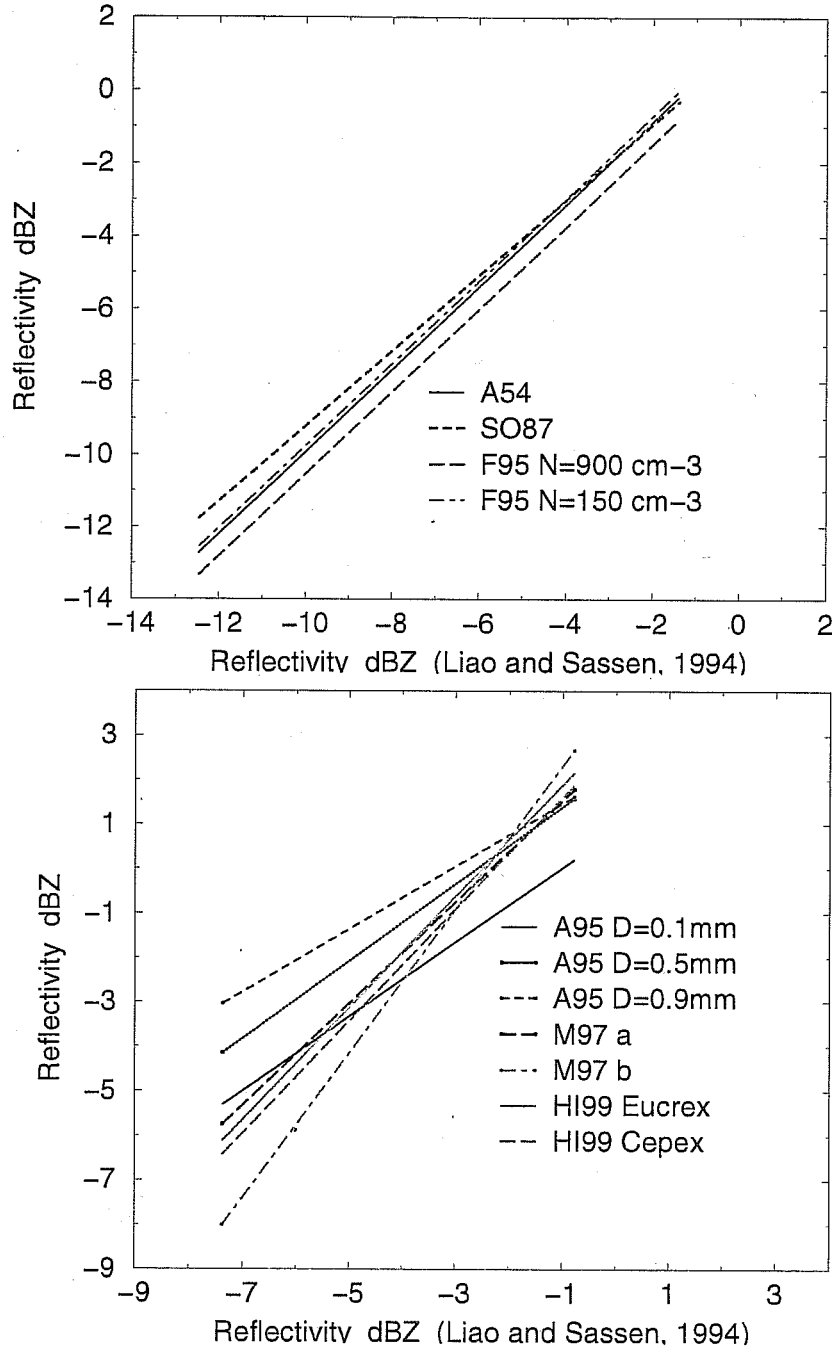

Figure A1: To facilitate the assessment of the agreement between different reflectivity parametrizations, the Ze reflectivities from different authors (see Table 8) are all plotted against the reflectivities of Liou and Sassen (1994): Ze-reflectivities for liquid water (top) and ice water clouds (bottom). Reflectivities are computed with published relationships from the liquid and ice water contents produced by the ECMWF model for April 1999.